Final Report

Project Title:	Aluminum epilayers for controlled growth and processing of high-efficiency, low-cost III-V solar cells
Project Period:	05/01/16 – 10/31/17
Project Budget:	$179,003 (Federal share), $26,356 (Non-Federal share)
Submission Date:	01/30/18
Recipient:	South Dakota School of Mines and Technology (SDSMT)
Address:	501 E. Saint Joseph St. Rapid City, South Dakota 57701-3901
Award Number:	DE-EE0007363
Project Team:	Rochester Institute of Technology (RIT) Lakewood Semiconductors (LkwdSemi)
Contacts:	Phil Ahrenkiel Professor Phone: 605-394-5238 Email: Phil.Ahrenkiel@sdsmt.edu

Executive Summary: The primary objective of the project was to develop $Ga_{0.82}In_{0.18}As$ (GaInAs) solar cells grown on epilayers of elemental Al. At this composition, GaInAs has a nearly optimal bandgap (1.16 eV) for a single-junction photovoltaic device. However, GaInAs lacks a convenient, lattice-matched substrate, restricting most investigations to metamorphic structures. The metal Al is, in fact, precisely lattice-matched to GaInAs in the orientation GaInAs (001)[100]||Al(001)[110]. At present, however, epi-ready Al substrates are not readily available commercially and are subject to oxidation. However, epitaxial Al buffer layers could enable control of defect generation, thermal and light management, and rapid epitaxial lift-off for ultrathin devices.

The primary method proposed for depositing Al epilayers used in this project was MOCVD. Using conventional MOCVD conditions, the release Al from its associated organic components using standard metalorganic precursors proved to be impossible. We therefore pursued RF generation for plasma enhancement within the MOCVD reactor to assist in precursor decomposition. This PE-MOCVD approach was essentially successful for Al deposition at low temperatures and pressures, resulting in elemental Al films on C-coated TEM grids, glass slides, GaAs substrates, and buffer layers of GaInAs, AlInAs, AlInP, and GaInP.

Unfortunately, the goal of obtaining epitaxial Al layers on III-Vs remained elusive throughout the project. However, various forms of crystallographic texturing of the Al films on III-V surfaces were demonstrated in this work. We found some influences of substrate orientation on the resulting film texturing. The uses of Ga- and In-rich surfaces to affect Al nucleation were also examined. Through our studies of Al texturing during growth on various substrate orientations, we observe a preference for Al [110] aligned with the GaAs in-plane <110> directions. More specifically, during Al growth under some conditions on vicinal (001) GaAs surfaces, an alignment of Al [110] with GaAs <110>A is preferred.

In parallel with efforts on Al epilayer deposition, work proceeded on optimization of metamorphic GaInAs epilayers, double heterostructures (DHs), and single-junction solar cells. Low threading dislocation densities $<10^5$ cm^{-2} and exceptionally long (~18 us) minority-carrier lifetimes resulted, leading to solar-cell device fabrication with conversion efficiencies of ~11%.

Table of Contents

Background:

Acronyms used

MOCVD	metalorganic chemical vapor deposition
PE-MOCVD	plasma-enhanced metalorganic chemical vapor deposition
TMAl	trimethylaluminum
TTBAl	tritertiarybutylaluminum
DMAlH	dimethylaluminum hydride
TMAAl	trimethylamine alane
SEM	scanning electron microscopy
AFM	atomic force microscopy
XRD	x-ray diffraction
TEM	transmission electron microscopy
STEM	scanning transmission electron microscopy
DH	double heterostructure
SRV	surface-recombination velocity
TRPL	time-resolved photoluminescence
RCPCD	resonant-coupled photoconductivity decay
EQE	external quantum efficiency
J-V	current-voltage
BF	bright field
DF	dark field
SE	secondary electron
SA or SADP	selected-area diffraction pattern
CB or CBED	convergent-beam electron diffraction
FFT	fast Fourier transform

Epitaxial Al

Specifications of the various orientations of Al relevant to this study are summarized in Table 1. The notation "Al(hkl)[uvw]||GaAs(hkl)[uvw]" indicates that the film crystallographic direction (hkl) (referenced to the reciprocal lattice) is parallel to the substrate normal direction (hkl), while a second film direction [uvw] (referenced to the direct lattice) is parallel to the substrate direction[uvw]. This second direction is most often taken to be parallel to the substrate plane.

Table 1.Specifications of Al orientations discussed in this work. Here GaAs could represent any cubic substrate material, such as GaAs, GaInAs, or AlAs.

name	specification	# of variants	comments
a001-I	Al(001)[100]||GaAs(001)[110]	1	targeted structure
a001-II	Al(001)[100]||GaAs(001)[100]	1	cubic alignment
a011	Al(011)[100]||GaAs(001)<110>	2	semi-epitaxial
a001-III	Al(001)[110]||GaAs($1\bar{1}1$)<110>	3	on (111)B substrate
a112	Al(112)[$1\bar{1}0$]||GaAs(110)[$\bar{1}$10]	1	on (110) substrate

Crystallographic texturing along the growth direction is readily assessed by powder XRD scans. The full orientation specification generally requires additional measurements, such RHEED (in MBE) or TEM. The available references provide varying levels of detail on the orientation resulting from a particular growth method. Even seemingly similar experimental procedures often appear to result in different outcomes when performed by different groups.

Epitaxial or textured Al growth on Si has been studied by several groups [1–8]. Al and Si have a lattice parameter ratio very close to the rational fraction ¾ . Thus, Al on Si films often exhibit crystallographic alignment. But Al is a group-III metal, and Al-containing III-V compounds have many uses in photovoltaics. In the a001-I orientation, with the Al crystal rotated 45º from the substrate about the (001) growth axis [Fig. 1], Al has a lattice mismatch is only 1.3% with respect to GaAs, which many previous investigations have considered to be negligible. This so-called “coincidence-site” lattice matching [9] offers a means to expand the palette of useable film/substrate combinations.

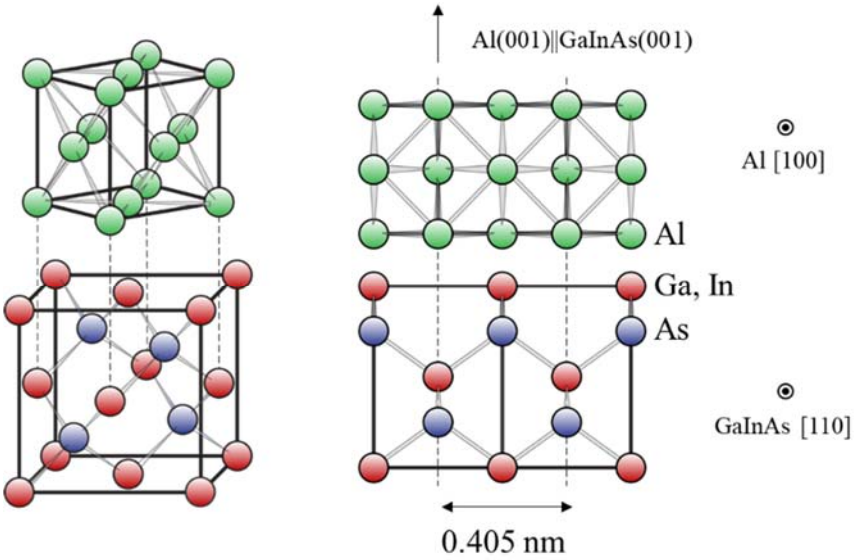

Fig. 1. Targeted a001-I epitaxial structure of Al on (001) GaInAs.

Al growth by MBE

The most successful attempts at epi-Al growth on III-V surfaces have been based on molecular-beam epitaxy (MBE). The first demonstration of epitaxial growth of Al on GaAs occurred at IBM in 1973 using MBE [10], only shortly after growth by the same group of the first AlGaAs/GaAs superlattices. The use of RHEED to study alternating Al/GaAs layers grown on (001) GaAs revealed a single variant in the a011 orientation. This indicates the formation of a “semi-epitaxial” heterointerface that is commensurate in only direction. It can be inferred that chemical effects at the growth surface in this system can be of comparable or greater importance than lattice-matching considerations.

Subsequent reports of epi-Al in both (011) and (001) orientations on GaAs (001) substrates can be found [11–16]. The use of single-crystal a001-I oriented Al on GaAs for Schottky-barrier diodes was demonstrated in 1978 [17]. A mixture of (011) and (001) orientations for Al on GaAs has been shown to tend towards (110) upon annealing [18].

Petroff et al. [19] reported a001-I epitaxy at high growth rates, although the films were described as rough and containing high dislocation densities.

A group at NREL reported epi-Al films produced by MBE on $MgAl_2O_4$ spinel substrates [20]. In a related patent [21], the use of these surfaces for GaInAs deposition are described, though only limited characterization data are presented.

Al growth by MOCVD

MOCVD is widely used for growth of epitaxial compound semiconductors with high purity, high yield, and high material quality, as well as precise growth control [22]. The deposition of Al-containing materials with high purity has been a challenge since the inception of MOCVD. In standard group-III alkyl precursors (e.g., TMAl and TTBAl), the metal is coordinated to C atoms within the organic component. Particularly in the case of Al-alkyls, these direct C bonds are not easily broken by pyrolysis. Oxygen (O) contamination can be a challenge for Al deposition by any method. Thus, both C and O incorporation have presented barriers to the widespread uses of Al-containing III-Vs in applications for which purity is a concern. To address this, several alternative Al precursors were developed that more readily decompose under typical growth conditions. DMAlH and TMAAl, for example, have no direct Al-C bonds, but do have other shortcomings involving their chemical stability and safety, as well as both cost and commercial availability. While growth of elemental Al films from alane-hydride and alkyl-alane precursors has had some success [23], growth of pure Al by conventional MOCVD from standard precursors has proven nearly impossible [24–26]. There is, therefore, considerable motivation to improve the release of Al from standard precursors.

The decomposition, or "cracking", of metalorganic and hydride precursors typically takes place by their exposure to high temperatures within a boundary layer surrounding the growth surface, with release of the constituent metal atoms or molecules into the vapor, along with the organic or hydrogen radical by-products. But the thermal energy at typical growth temperatures is insufficient to fully crack the Al-alkyl precursors [27]. III-V growth by MOCVD is most often performed with a vast excess of group-V hydride (e.g., PH_3, AsH_3), indicated by high V/III vapor flow ratios, which typically exceed 10 and can easily surpass 1000. It is the cracking of these hydride species at the growth surface that releases hydrogen radicals, which would not be present otherwise, even with an abundant flow of H_2 diluent. According to Stringfellow [22], these hydrogen radicals chemically react with the organic components of the group-III precursors, facilitating greater decomposition than would occur by thermal activation alone. Whereas a substantial portion of the metal components are typically incorporated into the solid film, the organic by-products are expelled to the exhaust.

PE-MOCVD

For CVD of group-IV materials (e.g., Si, Ge), hydrogen-plasma enhancement is commonplace, allowing higher growth rates and better crystallinity, and contributing to grain boundary passivation. But the use of PE-MOCVD of III-Vs is not widespread. Huelsman et al. [28,29] demonstrated the effect of plasma for abruptly switching on/off deposition during interfacial transitions for growth of GaPAs/GaAs multilayers, preventing transient overlap. A patent discussing PE-MOCVD of III-nitrides was filed [30] with no

experimental results. In the presence of plasma, growth can also be conducted at lower than normal temperatures, which can reduce interdiffusion.

The use of RF plasma to enable Al deposition from TMAl in H_2 on Si was reported by Masu et al. [31]. They reported good chemical purity and strong (001) orientation, but provided few structural details of the resulting films.

Plasma can be generated by several methods [32]. RF excitation provides a stable, controllable, and continuous plasma without requiring excessive system customization, such as vacuum feedthroughs. RF power from a generator is fed through an impedance matching network that is connected to an antenna coupled to the process. The RF antenna is often either capacitive, using parallel plates around the cavity vessel, or inductive, consisting of a copper coil wound around the vessel. Excitation results from the rapidly oscillating (13.56 MHz) electromagnetic fields in the cavity region imposed by the modulated voltage on the plates. The oscillating fields drive polarization of gas molecules, with a corresponding transfer of energy. As the temperature of the gas molecules rises, a portion of these atoms are ionized. An avalanche of free electrons is formed by collisions with remaining neutral atoms and ions, forming the plasma. A steady state is established once the free charge in the plasma is distributed to screen the applied field and limit a further degree of ionization.

Other influencing factors

The influences as templates for Al epitaxy of surfaces of various surface compositions have been explored in previous work. Yao et al. [33] suggested that AlAs surfaces have greater stability against decomposition, compared to GaAs surfaces. Growth on AlAs including incorporating thin Ga, In, and As surface layers to catalyze crystallization were studied by Maeda et al. [34]. Ga-terminated surfaces can be formed simply by heating a GaAs substrate without As overpressure [17].

GaInAs solar cells

Ultrathin GaAs currently holds the world record efficiency for a single-junction solar cell [35]. Metamorphic GaInAs subcells on GaAs form a common component of multi-junction devices [36], and GaInAs on InP has been considered for thermophotovoltaics [37,38]. However, relatively little work on single-junction GaInAs devices has been reported. Efficiencies of up to 16.3% in metamorphic GaInAs were demonstrated experimentally [39,40].

Introduction:

We adopted a plan based on targeted structures as follows [Fig. 2]: 1) Optimize GaInAs grades with respect to structural quality. Determine the composition profile and strain needed to produce an in-plan lattice parameter equal to that of unstrained $Ga_{0.82}In_{0.18}As$. 2) On this would be grown GaInAs/GaInP DHs for lifetime measurement, leading to further optimization. 3) Attempt metamorphic Al epitaxy by MOCVD directly on GaAs substrates. 4) Cap these structures with GaAs to evaluate GaAs/Al epitaxy. 5) Grow pseudomorphic Al epitaxial by MOCVD on a GaInAs displacement layer using a GaInAs grade. 6) On this grow a high-quality, pseudomorphic GaInAs layer. 7) Next grow GaInAs/GaInP DHs that incorporate the Al layer. Finally, produce 8) a companion GaInAs solar cell and 9) a GaInAs solar cell incorporating the Al layer.

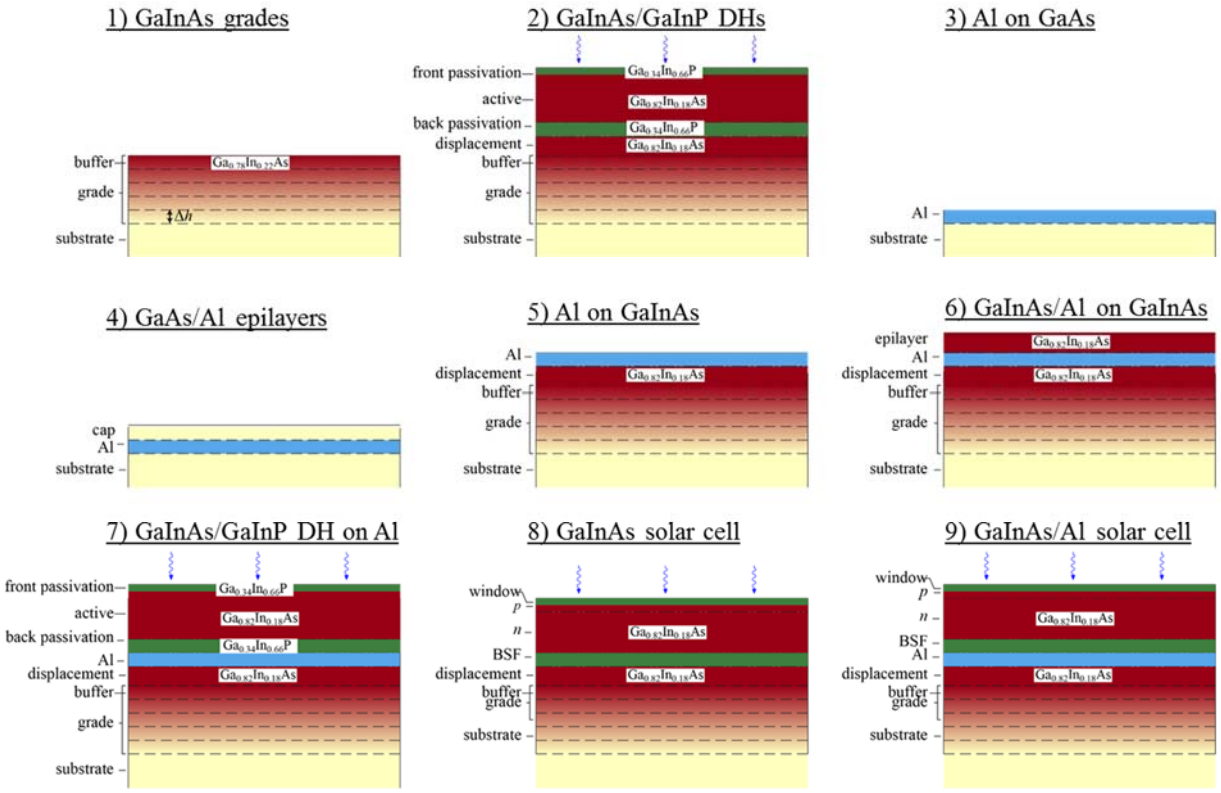

Fig. 2. Initial plan for structures to be grown during this project.

In the course of the project, we made progress on optimizing GaInAs grades and forming GaInAs/GaInP DHs to a point suitable for device applications. The bottleneck arose in depositing epi-Al by MOCVD. We attempted evaporation, and ultimately developed a method for Al deposition by PE-MOCVD. These Al films showed good texture, though epitaxy was not achieved. We therefore proceeded to fabricate GaInAs single-junction devices without epi-Al that shows efficiencies comparable to previous reports.

Project Results and Discussion:

GaInAs grades

GaInAs grades were grown at both SDSMT and RIT for comparison and to provide useful feedback between laboratories. We first studied uncapped grades to calibrate the strain at the top of the grade by XRD and characterize the dislocation distribution by TEM. These measurements confirmed that buried layers in a grade become more relaxed as subsequent steps in the grade are deposited, as expected, with decreasing dislocation density at the top surface.

We then proceeded to cap the grades with so-called “displacement”, or “fall-back”, layers of GaInAs, which are intended to form high-quality, low-strain templates, which serve to separate a DH or device from the graded region. TEM confirmed that these materials showed good structural quality, with little dislocation propagation to the free surface. A comparison of these structures was performed at RIT, in regard to growth conditions, grading rate, number of steps, and substrate misorientation (offcut) from (001). Four orientations were considered, as listed below. The various offcut directions can be inferred from an (001) pole figure. The influence of the offcut with regard to

surface composition is evident from <110> projections normal to the growth surface. On the (001) growth surfaces, steps are predominantly either of the (111)A type (cation terminated) or (111)B type (anion terminated). Offcuts towards <111>A create an abundance of A steps, whereas those towards <111>B create B steps [Fig. 3]. Offcuts towards any of the nearest <101> directions create a mixture of A and B steps. Although all <110> faces are non-polar, the in-plane <110> directions are often referred to as either <110>A or <110>B, which different in the polarity of nearest <111> direction.

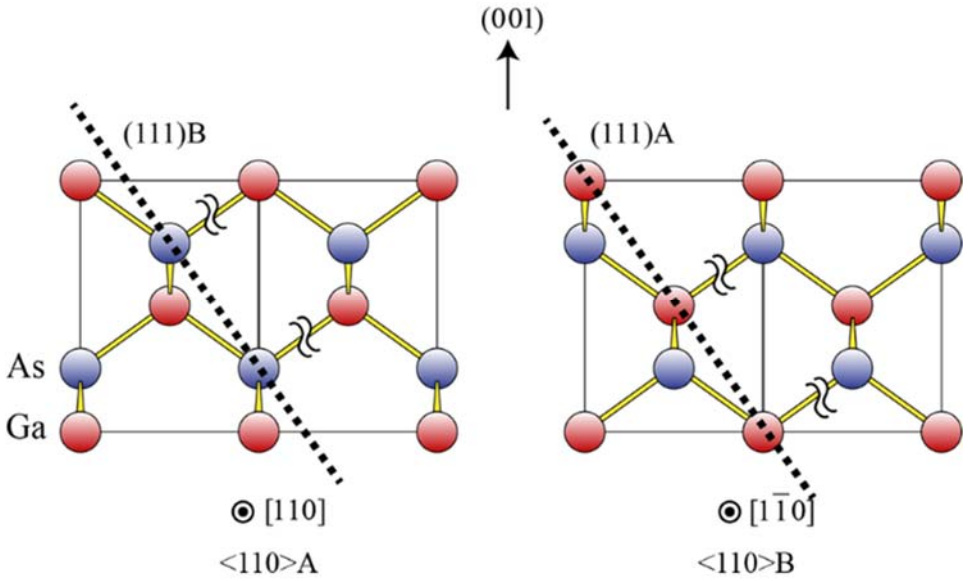

Fig. 3. <110>A and <111>B projections of GaAs. The (111)A and (111)B planes are distinguished with respect to the growth surface by cation (A) or anion (B) termination.

The particular GaAs substrate orientations used in this work and shorthand names are listed in Table 2:

Table 2. Substrate orientations related to this work.

orientation	abbreviation
GaAs oriented exactly on (001)	GaAs-0º
GaAs offcut *x*º from (001) towards <111>A	GaAs-*x*ºA
GaAs offcut *x*º from (001) towards <111>B	GaAs-*x*ºB
GaAs offcut *x*º from (001) towards <101>	GaAs-*x*ºAB
GaAs oriented exactly on (111)B	GaAs-111B
GaAs oriented exactly on (011)	GaAs-110

The A and B designations can be identified in the (001) stereographic projection for a cubic material. Various projections useful to distinguish substrate orientation and facilitate diffraction-pattern indexing are shown in Fig. 4.

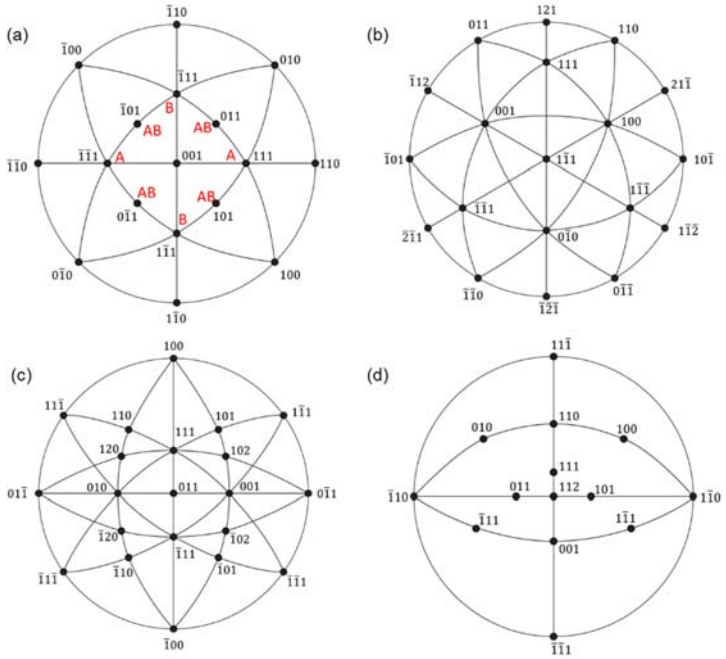

Fig. 4. <Stereographic projections of cubic materials along relevant zone axes: (a) (001); (1$\bar{1}$1); (c) (011); (d) (112). The A and B offcut directions for (001) III-V surfaces are shown in (a).

RIT generated detailed XRD reciprocal-space maps (RSMs) of graded samples using their Bruker system [Fig. 5]. We discussed issues of anisotropic strain relaxation, which become especially noticeable with offcut substrates. RIT adopted using 004, 224, and 2$\bar{2}$4 RSMs to explicitly identify this effect in the measurements.

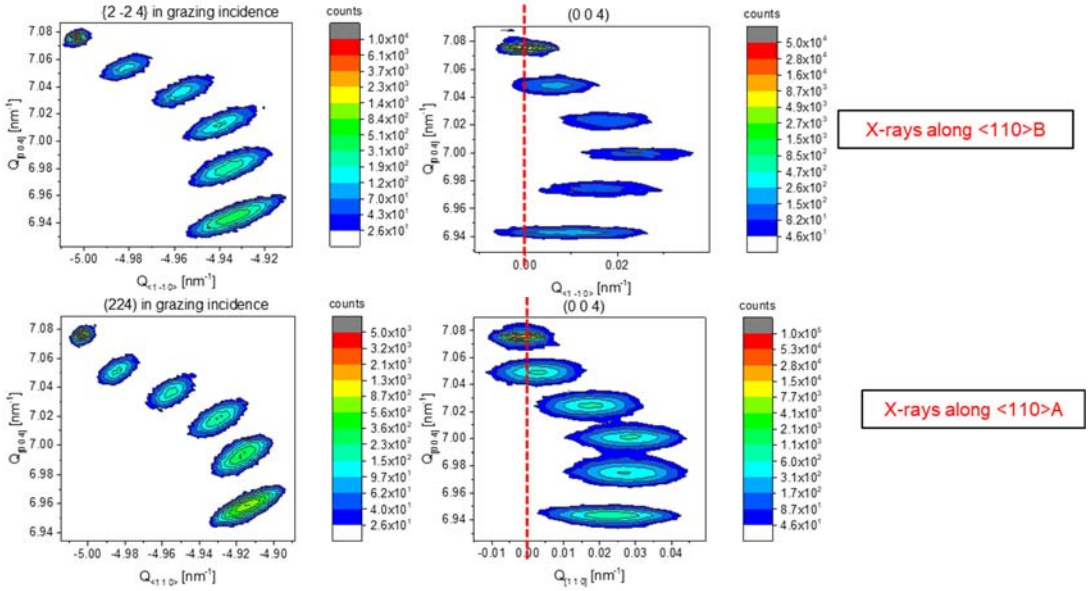

Fig. 5. XRD reciprocal-space maps of 004 and 224 peaks from GaInAs graded structures acquired in two orientations.

The same level of detail was not possible with the older Bede system at SDSMT. SDSMT primarily used 004 and 404 measurements, for which the anisotropy is

averaged out. Also, rather than using the full RSMs, which typically take several hours, we developed a procedure using a combination of rocking curves and $\Omega/2\theta$ scans to locate the maximum reflections for each layer. Analytical analysis shows that this is sufficient to accurately determine strain and composition, allowing calibration of gas flows for MOCVD [Fig. 6].

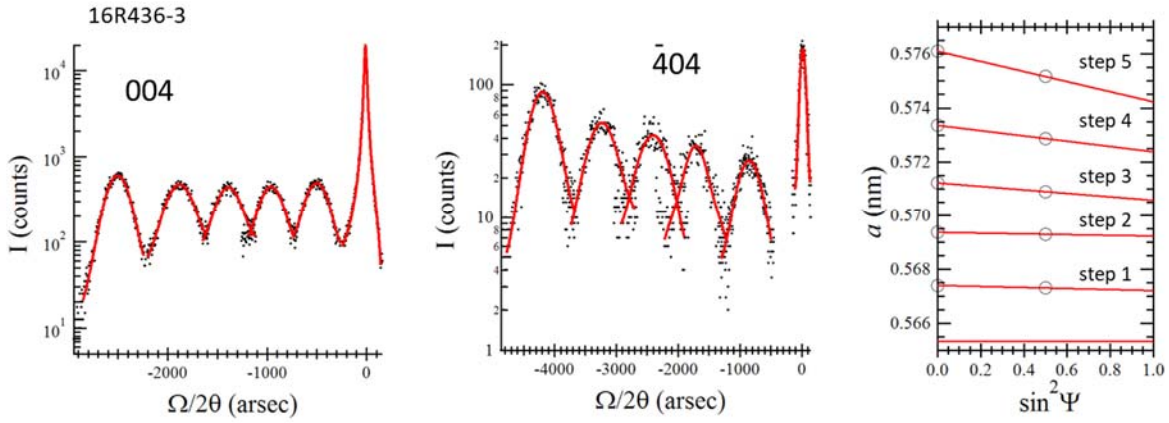

Fig. 6. XRD omega-2theta scans used of 004 and 404 peaks of GaInAs grades. An alignment procedure is applied to each layer to allow extraction of composition/strain from a linear fit.

TEM-EDX was used to further assess the composition profile. EDX maps acquired in STEM mode highlight the reduced In content in the displacement layer compared to the final step in the grade [Fig. 7]. Quantification of the alloy composition is possible using comparison to standards, but was not routinely performed, although EDX is necessary when characterizing higher-order (e.g., quaternary) alloys. The detailed dislocation morphology is best viewed in TEM 220-DF images.

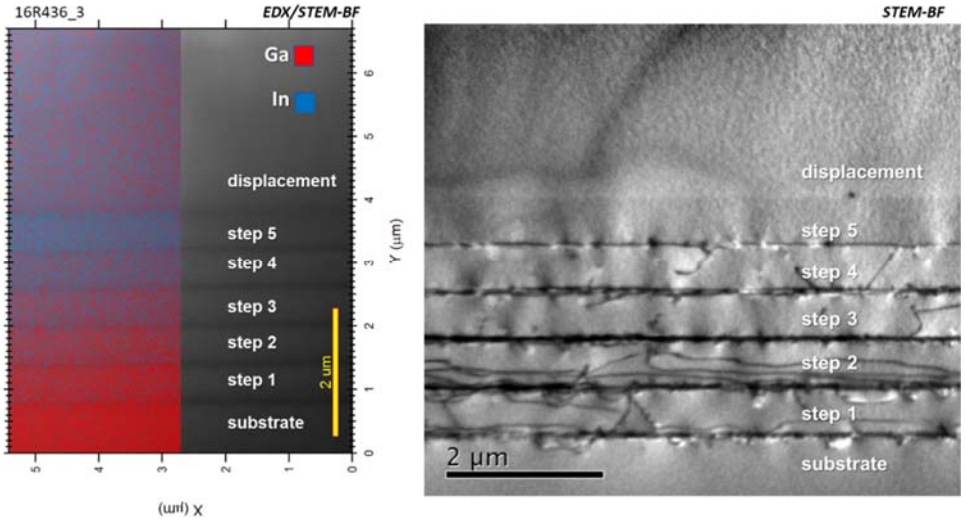

Fig. 7. STEM-EDX mapping of GaInAs graded structure.

The PL intensity and peak width of GaInAs grown using various growth temperatures, grade specifications, and vicinal (001) GaAs substrate orientations were used as metrics

for optimization. It was concluded that a growth temperature of 650 ºC, lower grading rate, smaller step size, and offcut of 6ºA gave the best emission spectra [Fig. 8].

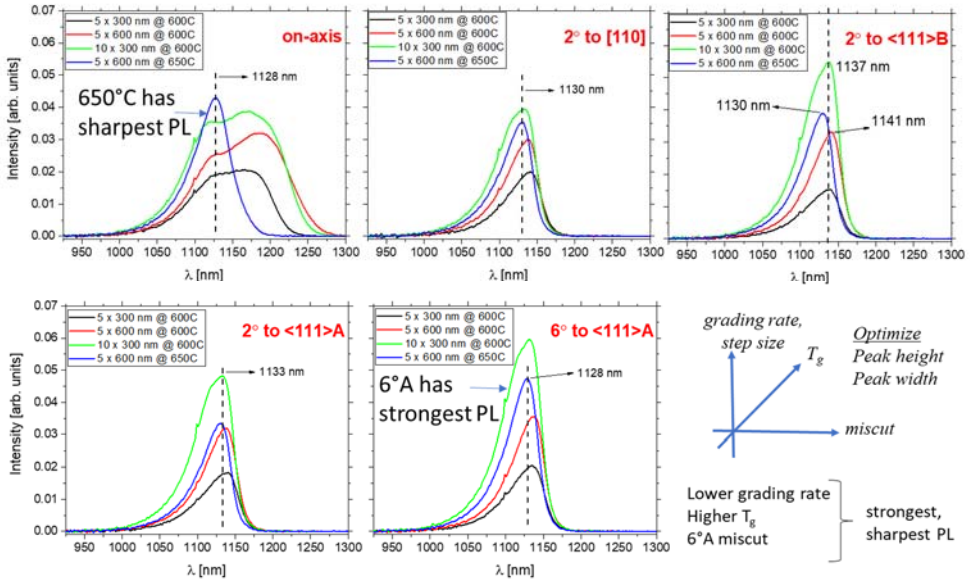

Fig. 8. PL spectra of GaInAs graded structures grown on various substrate orientations, at two different temperatures, with different grade designs.

Al growth

Al by conventional MOCVD

We initially attempted Al growth using conventional MOCVD on GaAs substrates to deposit layers of GaAs and GaInAs on an Al buffer layer formed while flowing TMAl only at 500-600 ºC. The films appeared rough and TEM analysis confirmed that the GaAs and GaInAs layers were polycrystalline. Though the buffer layers exhibited good definition and interface abruptness, the microstructures consisted primarily of an amorphous matrix in which were embedded very small (1-2 nm) nanocrystals [Fig. 9]. EDX analysis revealed high C content in the Al layers.

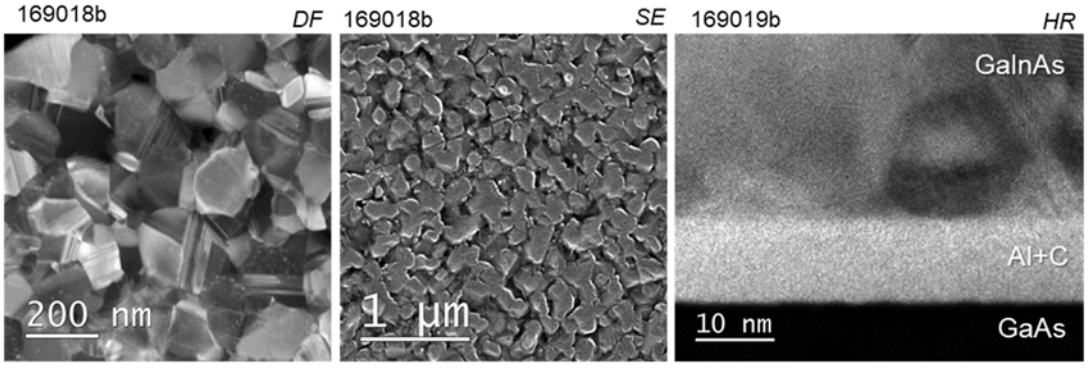

Fig. 9. Attempts to grow III-V/Al/III-V heterostructures using conventional MOCVD from TMAl.

The structures of these nanocrystals were not consistent with elemental Al. The showed a platelet-like structure inclined from the interface. Based on supporting powder XRD scans, we concluded that the dominant phase was rhombohedral Al_4C_3 [Fig. 10].

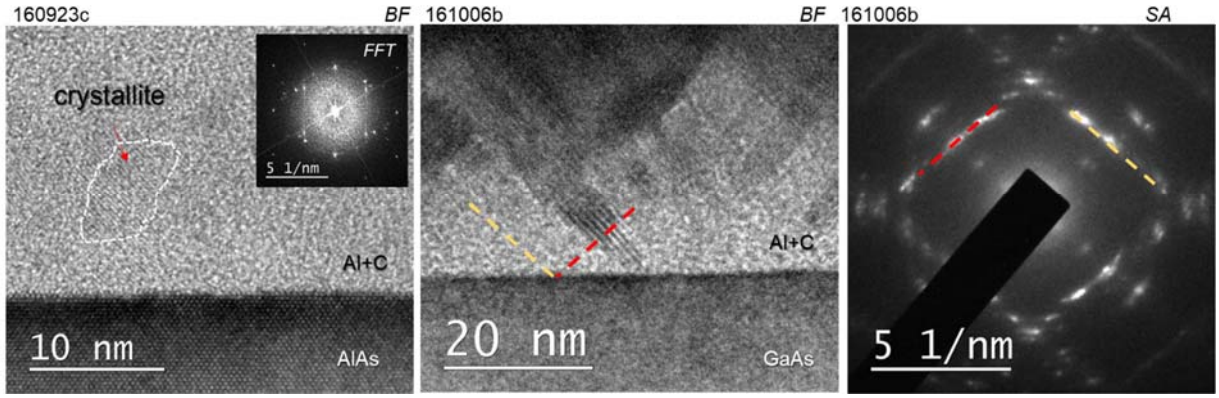

Fig. 10. Structure of Al+C layers that result from conventional MOCVD from TMAl.

Similarly, samples targeting Al epitaxy were grown at RIT using both TMAl and TTBAl precursors. Various buffer layers of GaAs, GaInAs, and AlAs were used to potentially affect Al nucleation. The targeted Al layers all appeared to consist of an Al_4C_3/a-AlC mixture. Those grown with TTBAl showed a relatively high degree of texturing in the orientation (001)[110]Al_4C_3||(001)[110]GaAs. The [110] in-plane orientation of the Al_4C_3 is clearly evident by strong 110 film peaks near the 220 substrate peaks when viewed in <110> cross-section. This places a component of the basal plane of the corresponding hexagonal unit cell parallel to the substrate plane, but rotational disorder appears to reduce alignment of the principal axis along the (001) growth direction. In all cases, GaAs and GaInAs films grown on these Al+C layers were polycrystalline [Fig. 11].

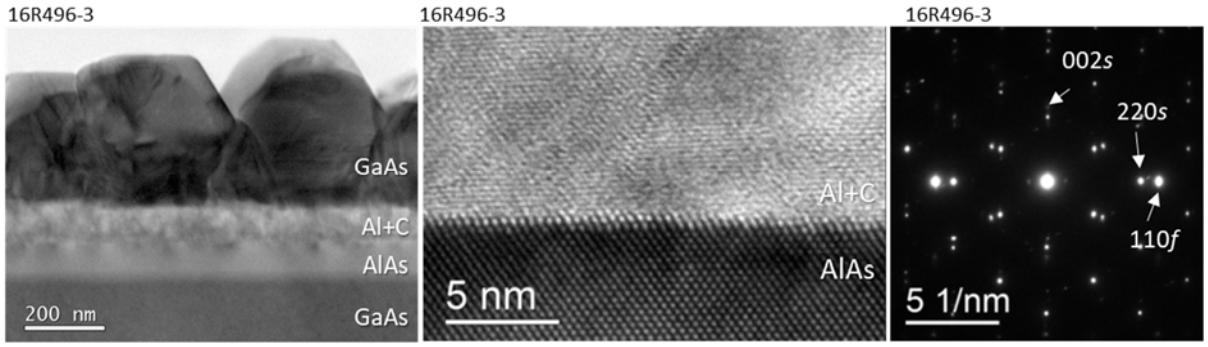

Fig. 11. Attempt at III-V/Al/III-V heterostructure by conventional MOCVD from TTBAl.

We performed MOCVD from TMAl under various conditions directly on C-coated TEM grids. Little deposition occurs below 500 ºC, whereas at high temperatures, the resulting material has a translucent, brown appearance. These were confirmed to consist primarily of Al_4C_3, in the form of platelets or whiskers [Fig. 12].

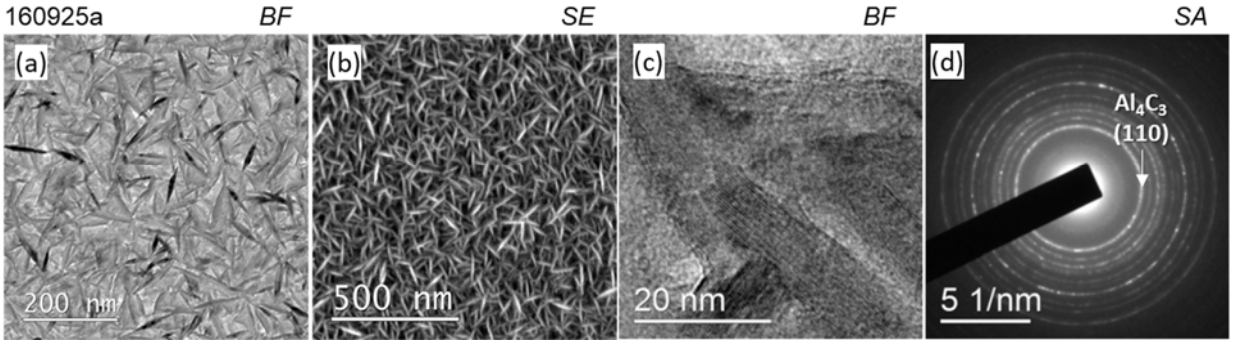

Fig. 12. MOCVD-grown Al-C film on TEM grid showing whisker or platelet-like Al_4C_3 features: (a) BF image; (b) SEM image; (c) BF image; (d) SADP. The Al_4C_3 (110) ring is highlighted.

Al by evaporation

Thermal evaporation of Al directly on TEM grids using a bell jar evaporator at SDSMT. Films deposited at room temperature contained Al grains on the order of tens of nm in size. We built a simple heating stage, using steel sheet and nichrome wire with alumina insulation, on which to mount samples within the evaporator. A significant increase to the micron scale in grain size was observed in films deposited at 300 ºC. These polycrystalline films were fairly rough [Fig. 13].

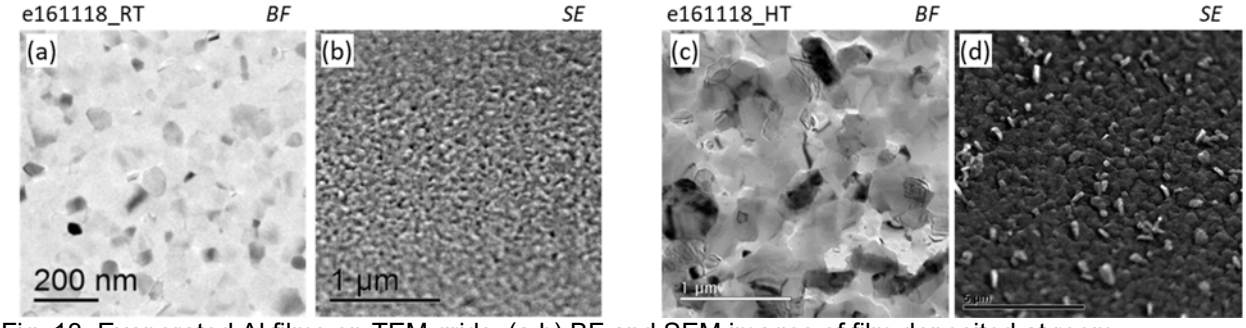

Fig. 13. Evaporated Al films on TEM grids: (a,b) BF and SEM images of film deposited at room temperature; (c,d) BF and SE images of film deposited at 300 °C.

The challenge remains to integrate these materials with MOCVD without exposing the air-sensitive Al films to atmosphere. We made only one attempt to evaporate Al directly on GaAs and Ge wafers, but no evidence of epitaxy resulted.

A flash evaporation system was used at RIT for deposition of Al buffer layers on which to grow GaInP/GaInAs DHs on GaInAs grades. This method also required an MOCVD growth interrupt to transfer the specimen for evaporation and characterization, then returning the specimen to the MOCVD system for subsequent growth [Fig. 14].

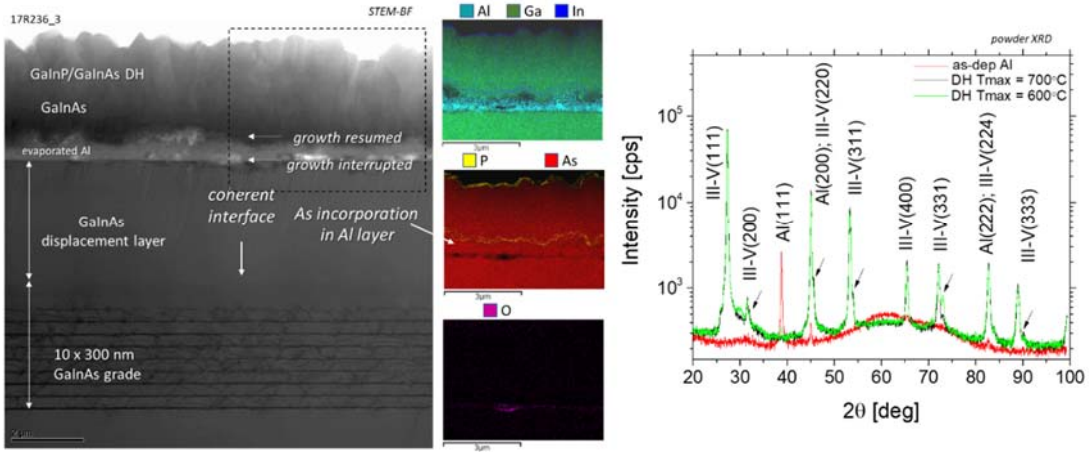

Fig. 14. Attempted GaInP/GaInAs DH on GaInAs grade using evaporated Al layer. As diffusion into the Al layer is detected by EDX. Powder XRD confirms that the Al layer and all subsequent layers are polycrystalline. The Al XRD peaks have diminished in intensity after subsequent deposition.

Attempted GaInP/GaInAs DH on GaInAs grade using evaporated Al layer. As diffusion into the Al layer is detected by EDX [41]. Powder XRD confirms that the Al layer and all subsequent layers are polycrystalline. The Al XRD peaks have diminished in intensity after subsequent deposition.

Al by PE-MOCVD

The PE-MOCVD antenna configuration was modified several times over the course of the project [Fig. 15]. Plasma was first generated within a quartz inlet tube roughly 20 cm away before the susceptor surface. We began with a horizontal, parallel-plate capacitive antenna shaped to conform to the tube (C). This was soon changed to an inductive coil wound around the tube (L1). Next, a coil was wound around the reactor neck (L2).

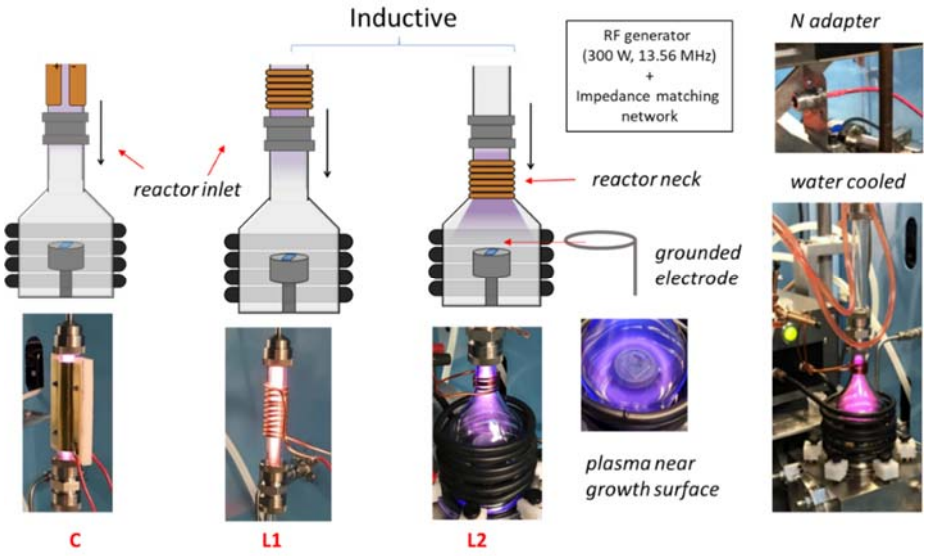

Fig. 15. PE-MOCVD configurations used: (C) capacitive on inlet; (L1) inductive on inlet; (L2) inductive on reactor neck. A grounded electrode was used to concentrate plasma near growth surface. A mounted N-style adapter was used to reduce impedance-mismatch losses. Water-cooled tubing was used to prevent antenna overheating.

A grounded electrode in the vicinity of the graphite susceptor was also considered to increase the plasma intensity at the growth surface, but the setup of the electrode is too cumbersome for routine use. Over time, we experienced failures of the connections between the coaxial cable supplying RF power and the antenna. Different adapter styles and water cooling of the antenna were then explored. We have also explored C/L hybrid antennae and vertical, axial, multi-plate capacitive antenna designs.

In initial PE-MOCVD growth runs from TMAl, we used configuration C, with a borrowed power supply and impedance-matching unit at relatively low RF power (30 W). Deposition was performed on Mo:C TEM grids at various T_g. At 600 °C and higher, the companion TEM grid showed a similar Al_4C_3 platelet structure to that observed without plasma. However, at 200 °C, the presence of larger clusters of elemental Al nanoparticles was observed [Fig. 16]. We encountered challenges in theses initial growth runs with substantial damage to the C support films during PE-MOCVD. Surviving clusters contained various shapes, including both rounded and faceted profiles, as well as straight needles. The crystal structure was confirmed by comparison of the electron-diffraction patterns with that from a common Al diffraction standard specimen. A thin oxide layer was evident on the surface of each Al nanoparticle.

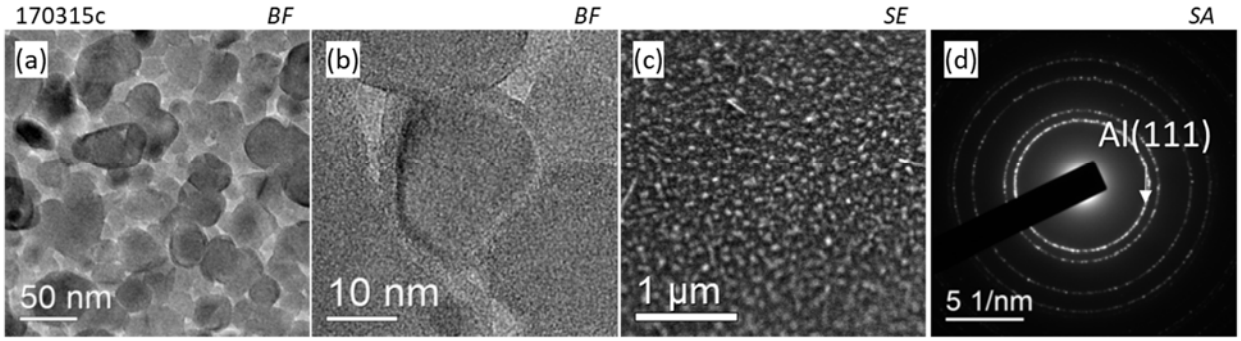

Fig. 16. PE-MOCVD Al on TEM grid: (a) BF image; (b) BF image; (c) SEM image; (d) SADP.

Next, we turned to Al on GaAs substrates. Used RF equipment was purchased for these experiments. The particular components were found to be easier to tune with an inductive antenna, using the L1 configuration. GaAs substrates offcut slightly from (001) were used in early stages for many of the samples for the particular reason that this simplified power XRD analysis. For example, the Al 220 Bragg angle is almost identical to that of the GaAs 004 (for the very reason that a001-I is targeted in the project.) In later stages of work, we realized that the substrate offcut has a strong influence on the resulting Al orientation. To specify the observed orientations identified by electron diffraction, we adopt the abbreviated convention in Table 3.

The initial Al films grown in the L1 geometry on GaAs-2ºAB appeared rough. Powder XRD showed texturing of approximately 50% (001) and 42% (110) in the first films of this type examined. The relative fraction f_j of orientation j was evaluated as

$$f_j = \frac{I_j / r_j}{\sum_i I_i / r_i}$$

where I_i and r_i are the measured and standard intensities for each refection i.

Table 3. Al orientations observed in this work. The a001(a) and a001(b) variants are referred to as (110) and (110)R in the literature.

name	variant	abbrev.	Notes
a011(a)	$Al(011)[0\bar{1}1]\|\|GaAs(001)[110]$	$f(1)$	(110) on (001) GaAs
a011(b)	$Al(011)[0\bar{1}1]\|\|GaAs(001)[1\bar{1}0]$	$f(2)$	(110)R on (001) GaAs
a001-II	$Al(001)[100]\|\|GaAs(001)[100]$	$f(3)$	(001) aligned on (001) GaAs
a001-III(a)	$Al(001)[110]\|\|GaAs(1\bar{1}1)[011]$	$f(4)$	(110) on (111)B GaAs
a001-III(b)	$Al(001)[110]\|\|GaAs(1\bar{1}1)[\bar{1}\bar{1}0]$	$f(5)$	"
a001-III(c)	$Al(001)[110]\|\|GaAs(1\bar{1}1)[10\bar{1}]$	$f(6)$	"
a112	$Al(112)[1\bar{1}0]\|\|GaAs(011)[0\bar{1}1]$	$f(7)$	(112) on (011) GaAs

Microscopic detail on the grain orientation was studied by TEM. The initial deposition of Al on a GaAs-2ºAB substrate showed a dominance of the orientation a001-II, rather than the a001-I variant targeted [Fig. 17]. Both a011 variants were also identified upon more careful inspection. The strong texturing is evident from the sharp electron-diffraction spots and their positions relative to the GaAs substrate spots. Additional spots in plan-view arise from double diffraction across the Al/GaAs interface [42].

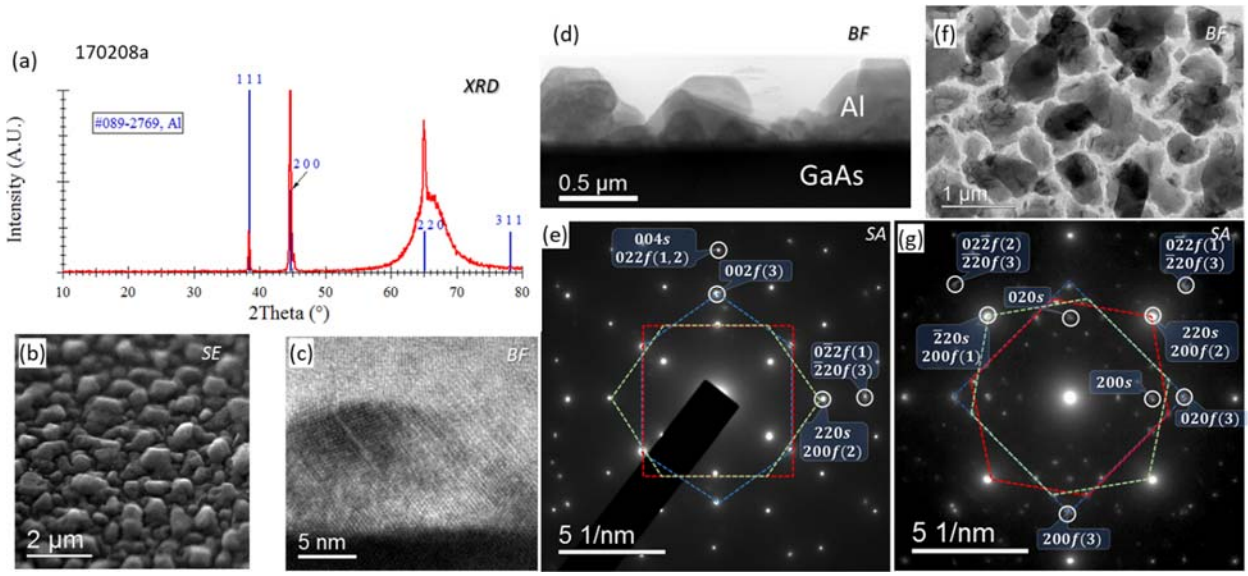

Fig. 17. Al on GaAs-2ºAB: (a) powder XRD scan; (b) SEM image; (c,d) cross-section BF images; (e) [110] cross-section SADP; (f) plan-view BF image; (g) plan-view [001] SADP through interface.

Using the L2 configuration, the growth rate substantially decreased, so that the films became much more specular and uniform, but this may be partly due to reduced thickness. TEM in both cross-section and plan-view revealed the two a011 variants, with no evidence of 001 orientations [Fig. 18]. AFM showed a surface roughness of ~5 nm. The Al grains were roughly columnar. A slight contrast at the Al/GaAs interface may indicate an interfacial phase. Powder XRD patterns showed a significant Al 220 peak, though the analysis is ambiguous due to the overlap with GaAs 004.

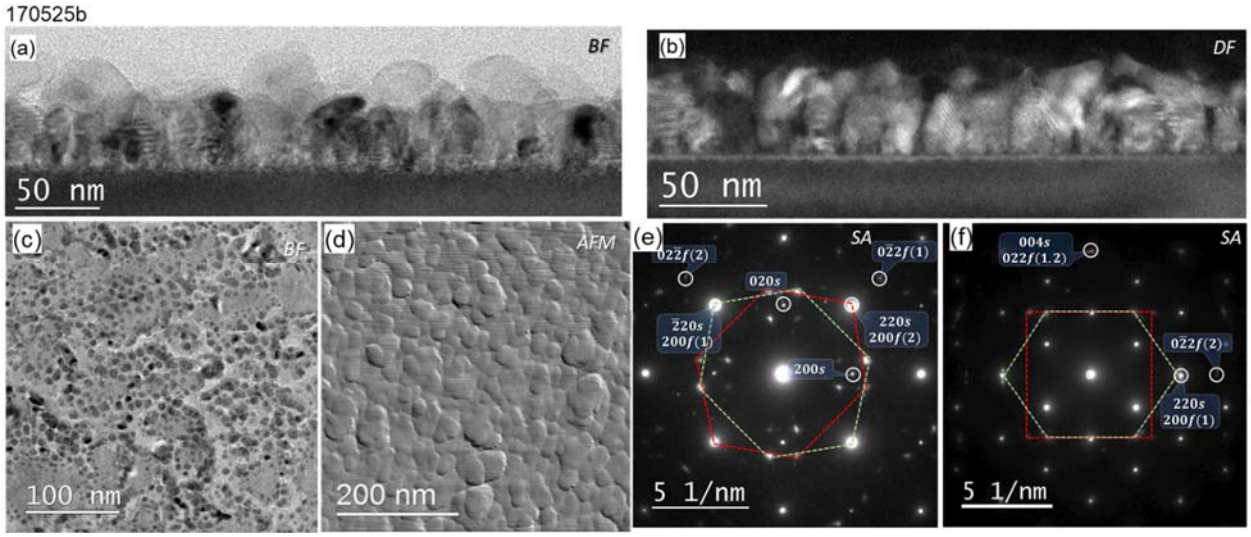

Fig. 18. Al on GaAs-0°: (a) BF image of cross-section; (b) DF image in cross-section; (c) BF image in plan-view; (d) AFM scan; (e) plan-view [001] SADP through interface; (g) cross-section [110] SADP along interface.

PE-MOCVD Al growth in the L2 PE-MOCVD configuration on (111)B-oriented GaAs substrate showed all three a001-III variants. Growth on a GaAs-011 substrate showed the single a112 variant [Fig. 19].

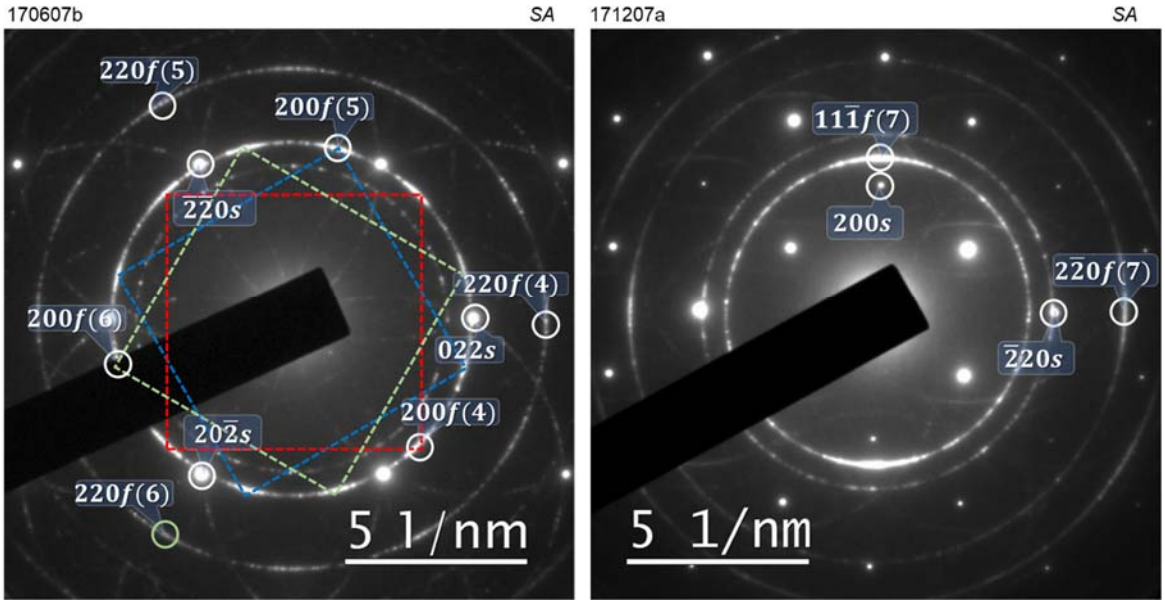

Fig. 19. Diffraction patterns taken in plan-view through interface regions from PE-MOCVD Al on GaAs: (a) [111]B pattern from Al on GaAs-111B; (b) [011] pattern from Al on GaAs-110.

The relevant orientations on (001) substrates are depicted in Fig. 20. Notice that the a001-II and a011 orientations each have at least one in-plane <110> direction for the film that is parallel to an in-plane <110> direction of the substrate.

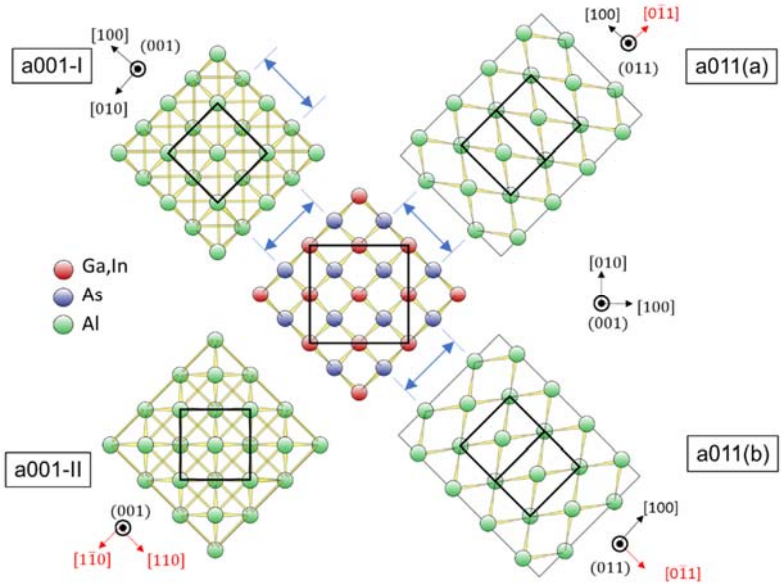

Fig. 20. Orientations of Al on (001) substrate. Only 001-I has not been observed. Aligned in-plane <110> directions of the film are shown in red.

We observed all three a001-III variants on GaAs-111B substrates [Fig. 21]. Again, notice that each of the variants has an in-plane <110> parallel to an in-plane <110> of the substrate.

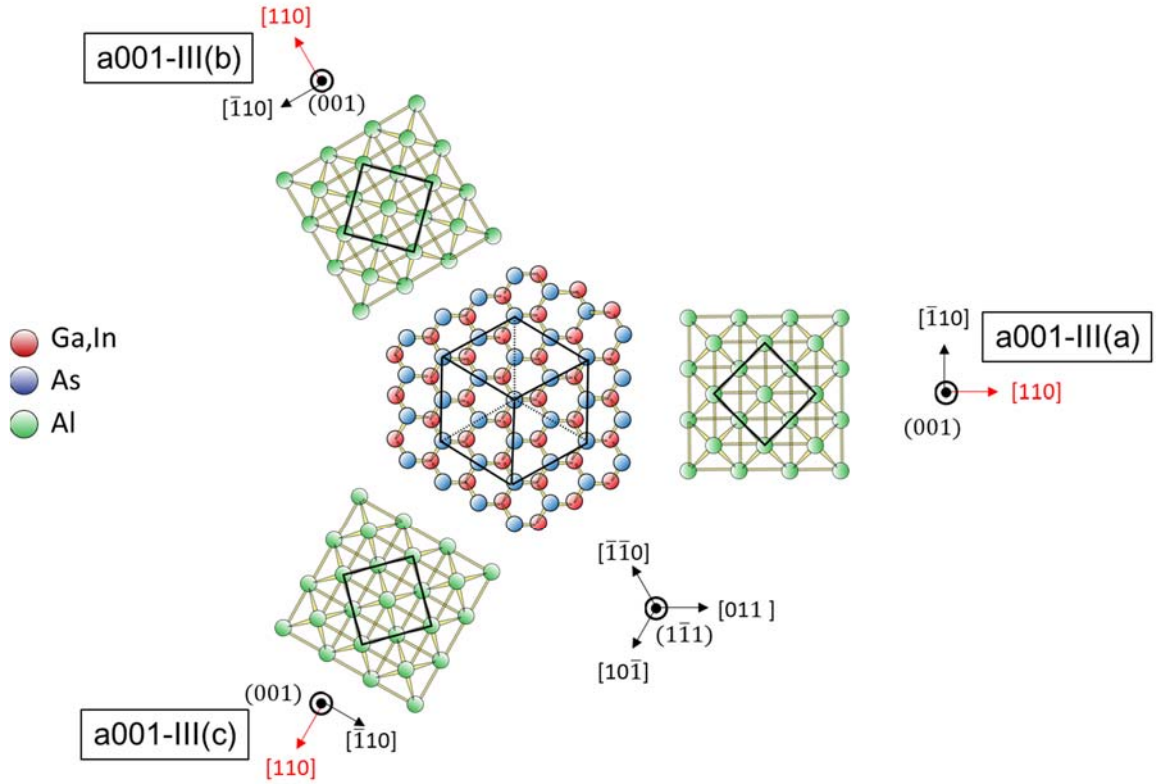

Fig. 21. Observed orientations of Al on GaAs-111B. Aligned in-plane <110> directions of the film are shown in red.

We observed the a112 orientation on GaAs-011 substrates [Fig. 22]. Again, notice that the Al in-plane <110> is parallel to the in-plane <110> of the substrate.

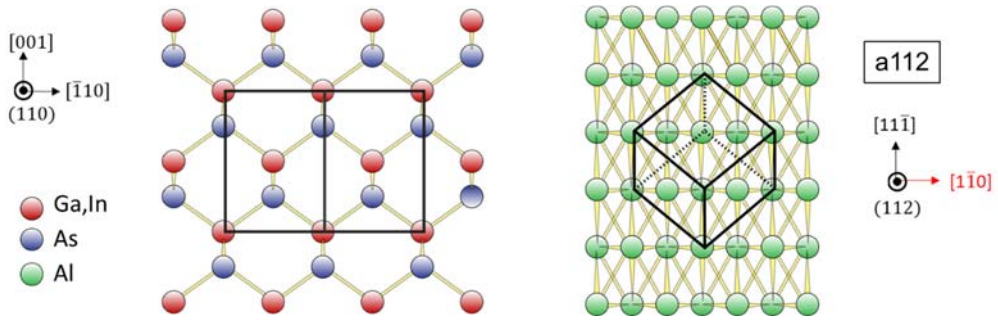

Fig. 22. Observed orientation of Al on GaAs-011. The aligned in-plane <110> direction of the film is shown in red.

This in-plane <110> alignment effect applies to all of the orientations we have observed experimentally, highlighting a potential influence on the preferred orientation.

Lastly, using an improved, water-cooled antenna in the L2 configuration, one of the two possible a011 variants was found to be strongly enhanced over the other, with the a001-II orientation also present [Fig. 23]. It is useful to identify which of the a011 variant is enhanced to understand the influence of surface orientation. Using the convergent-beam electron diffraction method [43] to identify the surface polarity, the dominant variant was found to be a011(a). This suppressed orientation has been referred to as (110)R [12].

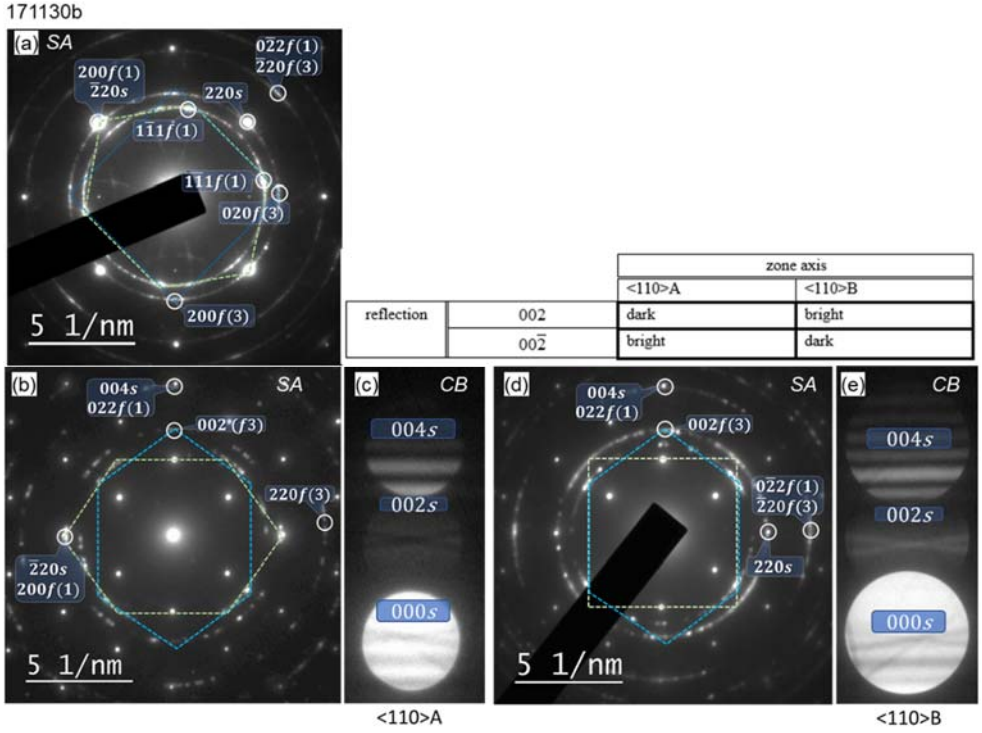

		zone axis	
		<110>A	<110>B
reflection	002	dark	bright
	$00\bar{2}$	bright	dark

Fig. 23. Diffraction data from PE-MOCVD Al on GaAs-2ºAB: (a) [001] PV; (b,c) [110]A cross-section and 002 CB spot; (d,e) [110]B cross-section and 002 CB spot. Contrast within the 002 spot is used to identify the orientation based on the table.

Catalyzed Al growth

Several experiments were performed to induce crystallization through the presence of Ga and In as metal catalysts. A challenge is controlling the dose of the catalyst metal during MOCVD. Plasma enhancement enables depositing these metals at relatively low temperatures. We repeatedly observed evidence of a thin, interfacial layer in these experiments (as well as in some samples that did not include intentional catalyst) [Fig. 24]. Often, the layer appeared to be epitaxial, but small grains were evident in others.

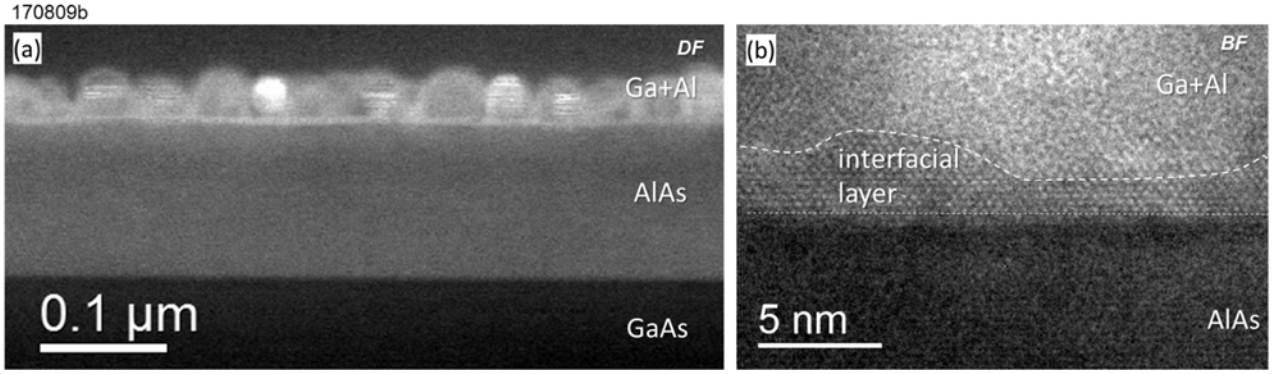

Fig. 24. TEM data from PE-MOCVD layer on AlAs using Ga catalysis. Large Ga+Al droplets form on the surface. An epitaxial interfacial layer was noticeable.

Al-C deposition

we hypothesized that improvement of the Al_4C_3 domain size could result in growth on (111) oriented cubic substrates. A deposition on GaAs-111B showed a strong (001) orientation, particularly evident from the (1,1,12) lattice planes and associated diffraction spot [Fig. 25]. As for Al deposition, the Al_4C_3 tends to orient with its in-plane (110) axis parallel to an in-plane (110) of the substrate. Nonetheless, the material remained highly defective, making it difficult to envision a practical application.

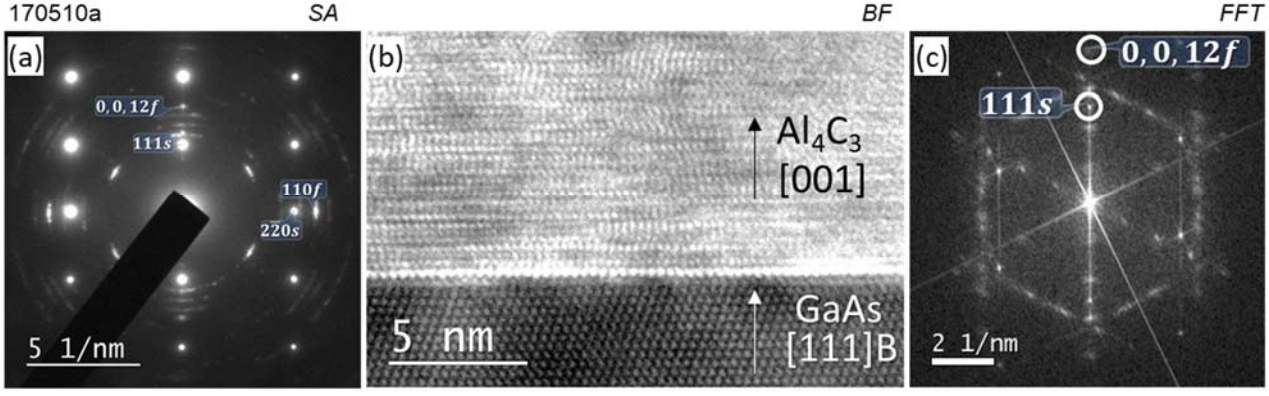

Fig. 25. Interface region of MOCVD grown Al_4C_3 on GaAs-111B: (a) <112> SADP; (b) <110> lattice image; (c) FFT of image in (b).

To study the ability to switch between Al and Al-C using PE-MOCVD, we grew structures with alternations between the two materials by changing growth temperature and switching plasma on/off [Fig. 26]. Although the Al_4C_3 structure was clearly evident in TEM data, it was difficult to confirm whether the intended Al layers did not contain significant amounts of C because of a large difference in ion-milling rates during sample prep.

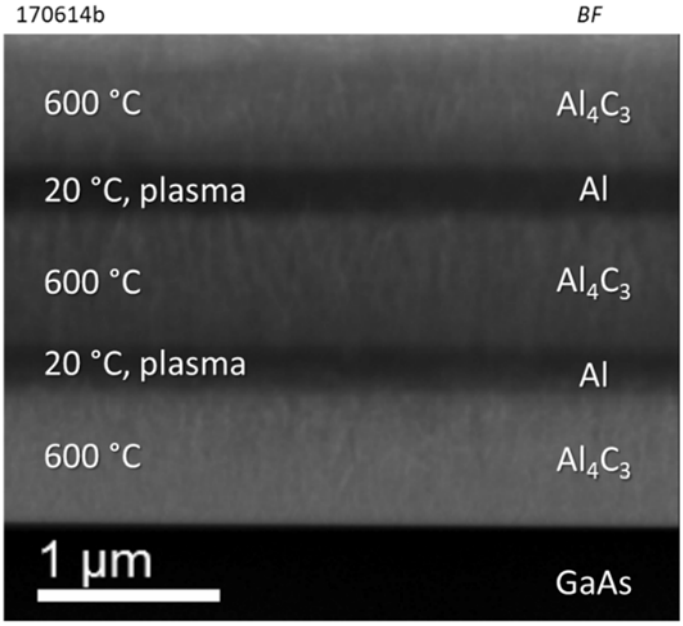

Fig. 26. Alternating Al-C/Al layers using MOCVD/PE-MOCVD.

Alternative surfaces

Growth of PE-MOCVD Al on an AlAs buffer on GaAs-2ºAB gave a dense, highly specular Al film, but with no evident texturing. It is well known that As will desorb from a GaAs surface above about 300 °C, requiring an As overpressure to be maintained at typical growth temperatures. PE-MOCVD of Al on GaInP, AlInP, and GaInAs surface was also performed [Fig. 27]. Only a few attempts were made of Al growth on the proposed GaInAs surfaces, due to the time demands of deposition. An optimized, metamorphic GaInAs graded structure from RIT on a 3" wafer was cleaved into several pieces to allow repeated attempts, though we only completed two growth runs in this mode.

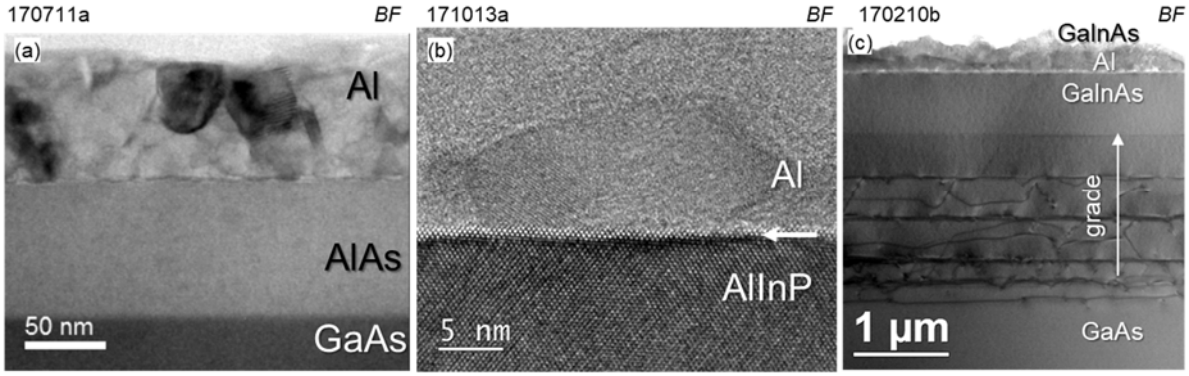

Fig. 27. PE-MOCVD Al on AlAs, AlInP, and GaInAs (with GaInAs cap).

GaInAs/GaInP DH lifetimes

RCPCD lifetimes on GaInAs/GaInP DHs were measured at LkwdSemi by RCPCD [Fig. 28]. Lifetimes of undoped samples were approximately 30 µs, indicating excellent structural and electronic quality.

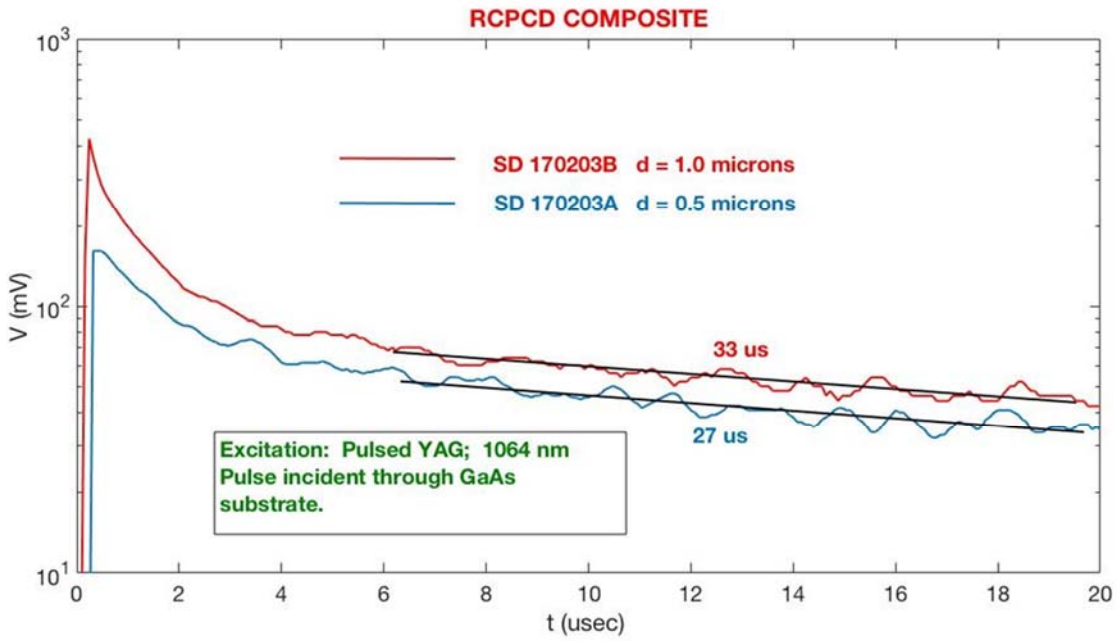

Fig. 28. RCPCD decay curves for two GaInAs/GaInP DHs grown at SDSMT.

The lifetimes of a set of samples doped with Si in the mid 10^{17} cm^{-3} range were too short for measurement by RCPCD. These were taken to NREL for TRPL by Steve Johnston [Fig. 29]. Lifetimes of ~20-35 ns indicate radiative recombination as the dominant mechanism.

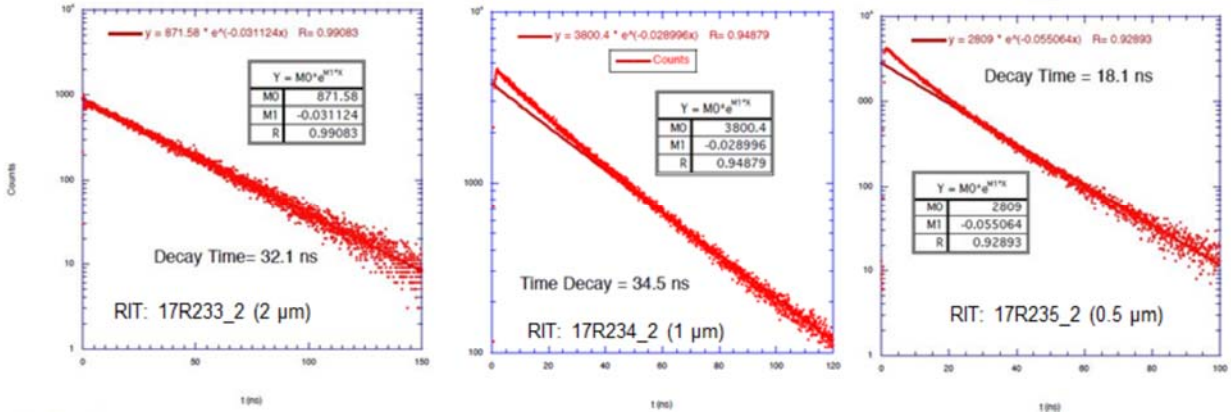

Fig. 29. TRPL decay curves for three DHs grown at RIT. (Data courtesy S. Johnston, NREL.)

GaInAs solar cells

RIT proceeded with growth of GaInAs solar cells. Device structures were grown on the metamorphic InxGa1-xAs buffers using Aixtron MOVPE; GaAs (001) substrates with off-cuts of 2º to (001), 6º to <111>A and 6º to <110> were utilized. The solar cell structures were grown at 650 ºC using diethylzinc and disilane as dopant precursors. Effects of the substrate offcut and grading scheme on the solar cells performance were studied. In addition, designs with thick (500 nm) and thin (200 nm) p-type emitter were tested. Two grading schemes were implemented for metamorphic buffer: one comprising 5 steps, each 600 nm-thick, and a finer one, with 10 steps by 300 nm; the corresponding In-fraction

variations were x = 0.04, 0.08, …, 0.18 and x = 0.02, 0.04, …, 0.18. The nomenclature of the samples produced with 3 different substrate offcuts, 2 different grading scheme and thin and thick emitter layers is given in [Table 4].

Table 4. Growth parameters varied among nine samples used for GaInAs solar cells.

	5 x 600 nm MMG		**10 x 300 nm MMG**
	200 nm emitter	**500 nm emitter**	**200 nm emitter**
2 deg. to (011)	2-200-5x	2-500-5x	2-200-10x
6 deg. to <111>A	6A-200-5x	6A-500-5x	6A-200-10x
6 deg. to <110>	6B-200-5x	6B-500-5x	6B-200-10x

1 cm x 1 cm solar-cell devices were fabricated using thermal evaporation for back and front contacts and isolated on the via mesa etch. Mesa etch depth was determined by the thickness of the active solar cell not including underlying metamorphic buffer.

The following process flow was used for solar cells fabrication:

Metallization was with the following process flow:

1. Au/Zn/Au front contact deposition by thermal evaporation
2. Mesa etch (concentrated HCl for GaInP; H_3PO_4:H_2O:H_2O 1:1:8 for GaInAs)
3. Contact etch
4. Ni/Ge/Au/Ni/Au back contact deposition by thermal evaporation
5. Annealing of contacts

Annealing of the contacts enabled diffusion and incorporation of additional dopants (Zn for p-type front and Ge for n-type back side) in the near-interface region of the solar cell contact layer promoting narrowing of the energy barrier occurring in a semiconductor material at a metal-semiconductor interface which facilitated tunneling of the charge carriers across the metal-semiconductor junction. This reduced contact resistance by up to 50 Ω as shown on Fig. 30 (b). No anti-reflective coatings were deposited on these devices [Fig. 30].

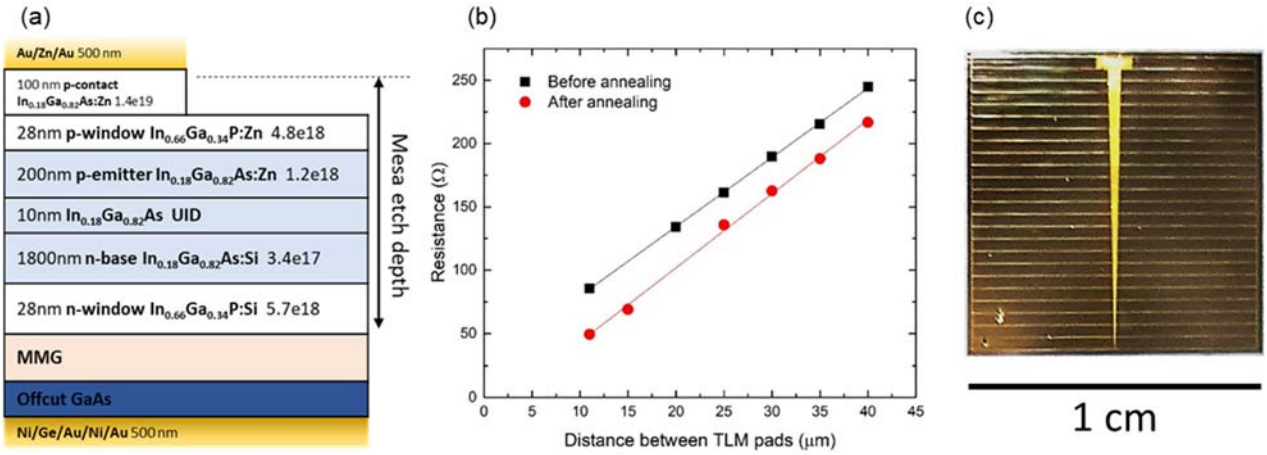

Fig. 30. GaInAs solar cells: (a) device structure; (b) electrical resistance before and after annealing; (c) photo of fabricated device.

The device heterostructures were grown using three different substrate orientations, two different grade designs, and two different emitter thicknesses

Devices were tested under AM1.5 G spectra [Fig. 31]. Efficiencies ranged from about 10-13 %, with the best device grown on GaAs-6ºB with a 5 x 600 nm grade using a 500-nm emitter. The most sensitive parameter in these devices was open circuit voltage (V_{oc}), as would be expected, since the metamorphic buffer will impact minority-carrier lifetime. The device with best V_{oc} was grown on GaAs-6ºB using a 10 x 300 nm grade using a 200-nm emitter. This device could possibly have been improved by increasing the emitter thickness as well, since clearly the emitter collection was not limited by the emitter diffusion length.

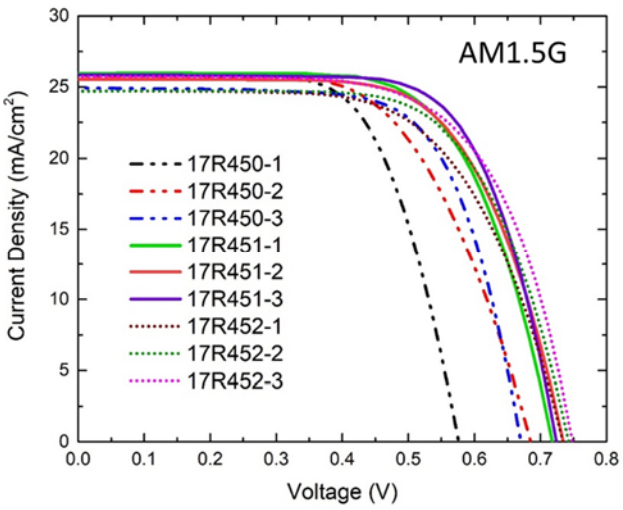

	V_{oc}, V	J_{sc}, $\frac{mA}{cm^2}$	FF, %	Eff, %
2-200-5x	0.576	25.9	66	9.8
6A-200-5x	0.686	25.7	61	10.8
6B-200-5x	0.671	24.9	68	11.4
2-500-5x	0.719	26.0	66	12.4
6A-500-5x	0.735	25.5	66	12.4
6B-500-5x	0.724	25.8	70	13.0
2-200-10x	0.734	24.7	63	11.4
6A-200-10x	0.743	24.7	67	12.2
6B-200-10x	0.749	25.8	65	12.6

Fig. 31. J-V characteristics of GaInAs devices. Device results are tabulated to the right. The highest efficiency value is circled.

EQE measurements were also performed and then simulated using Synopsys Sentaurus TCAD [Fig. 32]. Experimental EQE curves were fit with Sentaurus by tuning SRH minority

charge carrier lifetime and diffusion length [Fig. 31]. Extracted minority charge carrier (holes) SRH lifetimes in the base range from 10 to 20 ns to best match the data, which is also in agreement with TRPL measurements of these materials. An equation relating minority carrier diffusion length and threading dislocation density (Yamaguchi et al. [44]) provided an estimate of the threading dislocation density being in the order of 10^5 cm^{-2}, which represents relatively high quality metamorphic InGaAs.

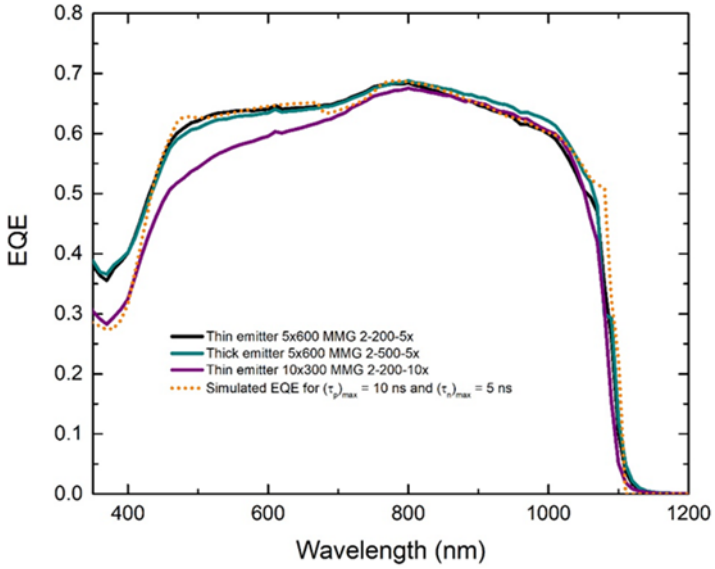

Fig. 32. EQE curves for three GaInAs devices and simulated EQE corresponding to the holes SRH lifetime of 10 ns.

Electrical properties of solar cells and their performance were found to be sensitive to the metamorphic buffer structures, substrate offcuts and emitter thickness [Fig. 33]. Larger offcut (6º) promotes higher open-circuit voltage, which would indicate a lower dislocation density and this lower rate of non-radiative recombination related to that defect density. The highest open-circuit voltages were measured on the samples with finer grading. These observations support PL analysis of the test metamorphic GaInAs samples.

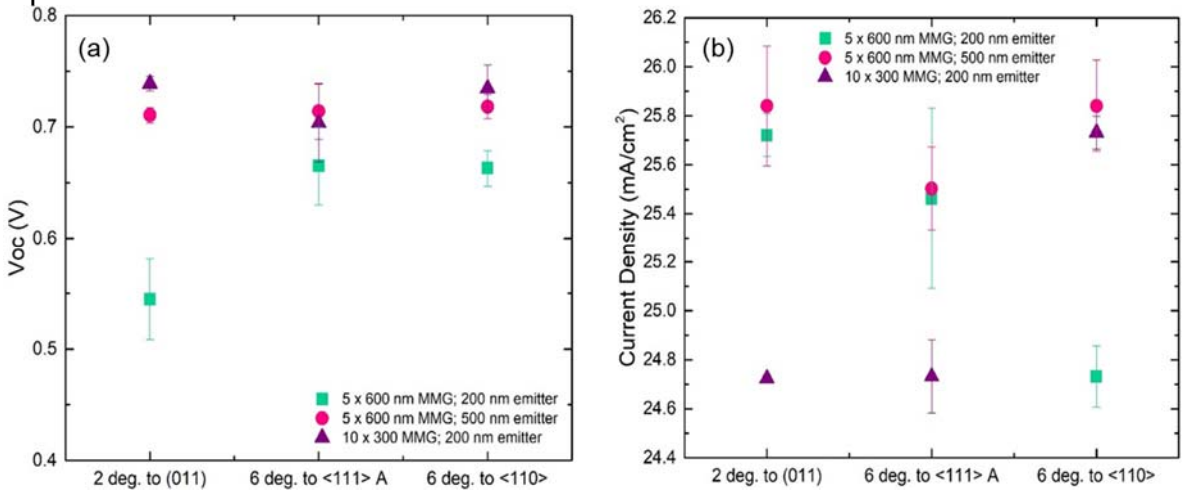

Fig. 33. Open-circuit voltages (a) and short-circuit currents (b) of GaInAs solar cells with thin and thick emitter and different grading schemes plotted vs. different substrate offcuts.

Maximum efficiencies calculated for the solar cells from each set of samples show several distinct trends [Fig. 34]. The offcut of 6ºAB was found to promote the highest efficiencies for all cells, reaching the maximum for the sample with thick p-type emitter. Both fine grading and thicker emitter promote an enhancement in efficiency. Increased thickness of the emitter improved overall device performance, likely due to improved emitter collection and lower dark current. This can be seen from the comparison of the results for V_{oc}, J_{sc}, and efficiency showing little variation with changing offcut.

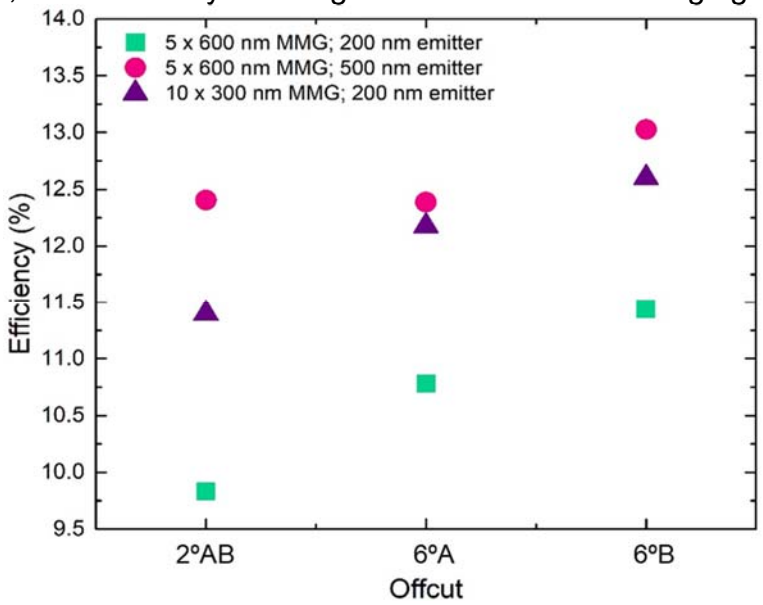

Fig. 34. Maximum efficiencies calculated for GaInAs solar cells plotted vs. different substrate offcuts.

Conclusions: Milestones were met only so far as high-quality GaInAs metamorphic layers were optimized and characterized, resulting in functioning solar cells. The initially proposed method of Al deposition did not prove tractable, due to C contamination. Alternative methods, such as evaporation, did not result in epi-Al films. The PE-MOCVD method was found to allow Al deposition in a manner consistent with the original intent of the proposal. Strong texturing of the resulting Al films was identified, but epitaxy remained elusive. A general description of the influences on Al texture on GaAs was proposed, in which an in-plane Al<110> tends to align with an in-plane GaAs<110>. Of the two <110> directions on vicinal (001) GaAs surfaces, it appears that the Ga<110>A is preferred under some conditions.

Budget and Schedule: The project budget consisted of a federal share of $179,003, with a recipient share of $26,356. A subward of $75,000 was made from SDSMT to RIT. SDSMT documented a total cost share of $17,832. RIT documented a total cost share of $8524.

The targeted May 1, 2016 start date was not met due to a delay in receipt of initial funds until Aug. 2016. A single NCE was allowed, extending the completion date to Oc. 31, 2017.

Path Forward: The PE-MOCVD method for Al deposition has opened a range of interesting problems to be addressed. The SDSMT group is determined to find a

broader understanding of the roles of growth orientation, chemistry, and conditions to control Al texturing and demonstrate epi-Al on III-Vs. SDSMT and RIT are pursuing joint funding on the use of Al in IV plasmonics. At photon energies exceeding 4 eV, the optical losses of Al are less than other noble metals, while the conductivity remains high. For this reason, recent studies have examined the enhancement of optical activity GaN and ZnO nanostructures on Al surfaces [45–48]. We are seeking support for an effort to continue improving Al layers, ultimately depositing widegap nanostructures on these metal layers. We have also demonstrated the use of PE-MOCVD for depositing GaN and AlN and are exploring its use for low-temperature deposition of III-V nanostructures with improved morphologies and interface abruptness.

Publications Resulting from This Work:1. A. Giussani, M. A. Slocum, S. M. Hubbard, N. Smaglik, N. Pokharel, and P. Ahrenkiel, "Integration of thin Al films on $In_{0.18}Ga_{0.82}As$ metamorphic grade structures for low-cost III-V photovoltaics" in *44th IEEE Photovoltaics Spec. Conf.* (Washington, DC, 2017) [41].

2. P. Ahrenkiel, N. Smaglik, N. Pokharel, A. Giussani, M. A. Slocum, and S. M. Hubbard, "Development of Aluminum Epilayers as Buffers for GaInAs" in *44th IEEE Photovoltaics Spec. Conf.* (Washington, DC, 2017) [42].

Accomplishments: The award enabled presentation at the *44th IEEE Photovoltaics Specialists Conference* of the two papers listed above [41,42]. Publication of the conference proceedings is in progress. A manuscript "Orientation and Microstructure of Al_4C_3 and Al films grown on GaAs Substrates" by the same authors is in preparation for submission to a peer-reviewed journal. An additional manuscript "Epitaxial recrystallization of Al deposited by plasma-enhanced MOCVD on GaAs", discussing recent work based on results of the project, is also in preparation. An abstract "Plasma-enhanced MOCVD for growth of elemental Al on III-V surfaces" has been accepted for presentation at the Materials Science & Technology 2018 conference.

The award supported one graduate student (Nikhil Pokharel) for one academic year while enrolled in the Nanoscience and Nanoengineering Ph.D. program at SDSMT.

The PI gave three interviews to local media regarding the project: An interview was held on the South Dakota Public Radio program *Innovation* on Aug. 12, 2016 (http://listen.sdpb.org/post/innovation-dr-phil-ahrenkiel). An interview on the project appeared in the Rapid City Journal on Jan. 4, 2017 (http://rapidcityjournal.com/news/local/mines-scientist-s-project-makes-solar-energy-s-future-bright/article_1d37e8a8-1aeb-569e-bfd6-64c6dd4daecc.html). A television interview appeared on KOTA News on Jan. 9, 2017 (http://www.kotatv.com/content/news/School-of-Mines-has-something-bright-in-research-410178955.html).

An invention disclosure "Plasma-enhanced metalorganic chemical vapor deposition of aluminum" by inventors S. P. Ahrenkiel and N. W. Smaglik was filed at SDSMT in July 25, 2017.

Disclaimer: This report was prepared as an account of work sponsored by an agency of the United States Government. Neither the United States Government nor any agency thereof, nor any of their employees, makes any warranty, express or implied, or

assumes any legal liability or responsibility for the accuracy, completeness, or usefulness of any information, apparatus, product, or process disclosed, or represents that its use would not infringe privately owned rights. Reference herein to any specific commercial product, process, or service by trade name, trademark, manufacturer, or otherwise does not necessarily constitute or imply its endorsement, recommendation, or favoring by the United States Government or any agency thereof. The views and opinions of authors expressed herein do not necessarily state or reflect those of the United States Government or any agency thereof.

Acknowledgement: This material is based upon work supported by the Department of Energy, Office of Energy Efficiency and Renewable Energy (EERE), under Award Number DE-EE0007363.

References:

[1] J. J. Lander, J. Morrison, and B. T. Laboratories, Surf. Sci. **2**, 553 (1964).

[2] N. Joshi, A. K. Debnath, D. K. Aswal, K. P. Muthe, M. S. Kumar, S. K. Gupta, and J. V. Yakhmi, Vacuum **79**, 178 (2005).

[3] T. Kobayashi, A. Sekiguchi, N. Hosokawa, and T. Asakami, Jpn. J. Appl. Phys. **27**, L1775 (1988).

[4] I. Levine, A. Yoffe, A. Salomon, W. Li, Y. Feldman, and A. Vilan, J. Appl. Phys. **111**, 124320 (2012).

[5] Y. Nakajima, K. Kusuyama, H. Yamaguchi, and Y. Murakami, Jpn. J. Appl. Phys. **31**, 1860 (1992).

[6] Y. Neo, T. Otoda, K. Sagae, H. Mimura, and K. Yokoo, Jpn. J. Appl. Phys. **37**, 2602 (1998).

[7] M. Sosnowski, S. Ramac, W. L. Brown, and Y. O. Kim, Appl. Phys. Lett. **65**, 2943 (1994).

[8] S. Yokoyama and K. Okamoto, Jpn. J. Appl. Phys. **30**, 3685 (1990).

[9] S. Kaneko, K. Akiyama, T. Ito, M. Yasui, M. Soga, Y. Hirabayashi, H. Funakubo, and M. Yoshimoto, Jpn. J. Appl. Phys. **49**, 2 (2010).

[10] R. Ludeke, L. L. Chang, and L. Esaki, Appl. Phys. Lett. **23**, 201 (1973).

[11] G. Landgren, R. Ludeke, and C. Serrano, J. Cryst. Growth **60**, 393 (1982).

[12] S. J. Pilkington and M. Missous, J. Cryst. Growth **196**, 1 (1999).

[13] P. Bhattacharya, J. E. Oh, J. Singh, D. Biswas, R. Clarke, W. Dos Passos, R. Merlin, N. Mestres, K. H. Chang, and R. Gibala, J. Appl. Phys. **37**, 3700 (1990).

[14] S. W. Lin, J. Y. Wu, S. Di Lin, M. C. Lo, M. H. Lin, and C. Te Liang, Jpn. J. Appl. Phys. **52**, 1 (2013).

[15] S.-T. Lo, C. Chuang, S.-D. Lin, K. Y. Chen, C.-T. Liang, S.-W. Lin, J.-Y. Wu, and M.-R. Yeh, Nanoscale Res. Lett. **6**, 102 (2011).

[16] B. Tadayon, S. Tadayon, M. G. Spencer, G. L. Harris, L. Rathbun, J. T. Bradshaw, W. J. Schaff, P. J. Tasker, and L. F. Eastman, Appl. Phys. Lett. **53**,

2664 (1988).

[17] A. Y. Cho and P. D. Dernier, J. Appl. Phys. **49**, 3328 (1978).

[18] H. F. Liu, S. J. Chua, and N. Xiang, J. Appl. Phys. **101**, 53510 (2007).

[19] P. M. Petroff, L. C. Feldman, A. Y. Cho, and R. S. Williams, J. Appl. Phys. **52**, 7317 (1981).

[20] Y. Lin, A. G. Norman, W. E. Mcmahon, H. R. Moutinho, C. Jiang, and A. J. Ptak, J. Vac. Sci. Technol. B **29**, 03C128 (2014).

[21] A. Ptak, T. Lin, A. Norman, and K. Alberi, US9041027 B2 (2015).

[22] G. B. Stringfellow, *Organometallic Vapor-Phase Epitaxy*, 2nd ed. (Academic Press, San Diego, 1999).

[23] T. Mitsui, E. Hill, R. Curtis, and E. Ganz, Phys. Rev. B **59**, 8123 (1999).

[24] A. C. Jones, J. Auld, S. A. Rushworth, and G. W. Critchlow, J. Cryst. Growth **135**, 285 (1994).

[25] J. J. Hill, A. A. Aquino, C. P. A. Mulcahy, N. Harwood, A. C. Jones, and T. S. Jones, Surf. Sci. **340**, 49 (1995).

[26] M. L. Geen, R. A. Levy, R. G. Nuzzo, and E. Coleman, Thin Solid Films **114**, 367 (n.d.).

[27] N. Suzuki, C. Anayama, K. Masu, K. Tsubouchi, and N. Mikoshiba, Jpn. J. Appl. Phys. **25**, 1236 (1986).

[28] A. D. Huelsman, L. Zien, and R. Reif, Appl. Phys. Lett. **52**, 726 (1988).

[29] A. D. Huelsman, R. Reif, and C. G. Fonstad, Appl. Phys. Lett. **50**, 206 (1987).

[30] K. Brown, K. Griffin, D. Bour, and O. Kryliouk, US0258580 A1 (2012).

[31] K. Masu, K. Tsubouchi, N. Shigeeda, T. Matano, and N. Mikoshiba, Appl. Phys. Lett. **56**, 1543 (1990).

[32] F. F. Chen, in *Adv. Plasma Technol.*, edited by R. D'Agostino, P. Favia, Y. Kawai, H. Ikegami, N. Sato, and F. Arefi-Khonsari (Wiley-VCH, 2007), pp. 99–115.

[33] T. Yao, H. Nakahara, H. Matuhata, and Y. Okada, J. Cryst. Growth **111**, 221 (1991).

[34] N. Maeda, M. Kawashima, and Y. Horikoshi, J. Appl. Phys. **74**, 4461 (1993).

[35] B. M. Kayes, H. Nie, R. Twist, S. G. Spruytte, F. Reinhardt, I. C. Kizilyalli, and G. S. Higashi, in *37th Photovoltaics Spec. Conf.* (Seattle, WA, 2011).

[36] W. T. Dietze, M. J. Ludowise, and P. E. Gregory, Appl. Phys. Lett. **41**, 984 (1982).

[37] P. Jurczak, A. Onno, K. Sablon, and H. Liu, Opt. Express **23**, A1208 (2015).

[38] M. W. Wanlass, J. S. Ward, K. A. Emery, M. M. Al-Jassim, K. M. Jones, and T. J. Coutts, Sol. Energy Mater. Sol. Cells **41/42**, 405 (1996).

[39] S. Katsumoto, A. Yamamoto, and M. Yamaguchi, Jpn. J. Appl. Phys. **24**, 636

(1985).

[40] R.-H. Horng, F. Wu, S. Ou, Y. Kao, and S. Shih, in *43rd IEEE Photovolt. Spec. Conf.* (Portland, OR, 2016), pp. 2341–2343.

[41] A. Giussani, M. A. Slocum, S. M. Hubbard, N. Smaglik, N. Pokharel, and P. Ahrenkiel, in *44th Photovolt. Spec. Conf.* (Washington, DC, 2017).

[42] P. Ahrenkiel, N. Smaglik, N. Pokharel, A. Giussani, M. A. Slocum, and S. M. Hubbard, in *IEEE Photovoltaics Spec. Conf.* (Washington, DC, 2017).

[43] J. Taftø and J. C. H. Spence, J. Appl. Crystallogr. **15**, 60 (1982).

[44] M. Yamaguchi and C. Amano, J. Appl. Phys. **58**, 3601 (1985).

[45] Y.-C. Chung, P.-J. Cheng, Y.-H. Chou, B.-T. Chou, K.-B. Hong, J.-H. Shih, S.-D. Lin, T.-C. Lu, and T.-R. Lin, Sci. Rep. **7**, 39813 (2017).

[46] B. Chou, Y. Chou, Y. Wu, Y. Chung, and W. Hsueh, Sci. Rep. **6**, 19887 (2016).

[47] M. W. Knight, N. S. King, L. Liu, H. O. Everitt, P. Nordlander, and N. J. Halas, ACS Nano **8**, 834 (2014).

[48] Q. Zhang, G. Li, X. Liu, F. Qian, Y. Li, T. C. Sum, C. M. Lieber, and Q. Xiong, Nat. Commun. **5**, 4953 (2014).